Inorganica Chimica Acta, 210 (1993) 107–124

Crystal structures, vibrational and ^{31}P NMR studies of complexes of tertiary phosphine ligands with mercury(II) halides

Graham A. Bowmaker*

Department of Chemistry, University of Auckland, Private Bag 92019, Auckland (New Zealand)

Howard J. Clase

Department of Chemistry, Memorial University of Newfoundland, St. Johns, Nfld., A1B 3X7 (Canada)

Nathaniel W. Alcock

Department of Chemistry, University of Warwick, Coventry CV4 7AL (UK)

Janet M. Kessler and John H. Nelson*

Department of Chemistry, University of Nevada, Reno, NV 89557-0020 (USA)

James S. Frye**

Department of Chemistry, Colorado State University, Fort Collins, CO 80523 (USA)

(Received March 2, 1993)

Abstract

The mercury(II) phosphine complexes $(R_3P)_2HgX_2$ ($R_3P=PPh_3$, PEt_3, 1-phenyldibenzophosphole (DBP), 1-phenyl-3,4-dimethylphosphole (DMPP); X = Cl, Br, I and PBu_3; X = Cl) have been prepared and their solution and solid state structures determined by a combination of elemental analyses, IR, Raman and NMR spectroscopy. The structures of $(DBP)_2HgBr_2$ (**1**), $(PPh_3)_2Hg_2Br_4$ (**2**), $(DMPP)_2Hg_2I_4$ (**3**) and $(Bu_3P)_2Hg_2I_4$ (**4**) have been determined from three-dimensional X-ray data collected by counter methods. Compound **1** crystallizes in space group $P\bar{1}$ with $a=10.568(6)$, $b=17.390(6)$, $c=9.610(3)$ Å, $\alpha=106.02(4)$, $\beta=100.62(4)$, $\gamma=101.41(5)°$ and $Z=2$. Compound **2** crystallizes in space group $P2_1/a$ with $a=18.619(7)$, $b=10.938(4)$, $c=18.762(5)$ Å, $\beta=90.36(2)°$ and $Z=4$. Compound **3** crystallizes in space group $Pbc2_1$ with $a=8.516(4)$, $b=19.404(7)$, $c=19.545(6)$ Å and $Z=4$. Compound **4** crystallizes in space group $P2_1/c$ with $a=16.450(16)$, $b=20.609(21)$, $c=24.263(31)$ Å, $\beta=109.38(8)°$ and $Z=8$. Compound **1** deviates from ideal C_2 symmetry having slightly different Hg–Br (2.618(2), 2.604(2) Å) and Hg–P (2.513(3), 2.490(3) Å) bond distances. The inequivalence of the phosphines is manifested as a second order ABX CP/MAS $^{31}P\{^1H\}$ NMR spectrum for **1**. Compound **2** is a symmetric doubly bromide bridged dimer with essentially equivalent Hg–P (2.40(2), 2.44(2) Å) bond distances but its CP/MAS $^{31}P\{^1H\}$ NMR spectrum displays two AX resonances, showing that the phosphines are not magnetically equivalent. Compound **3** is a symmetric, doubly iodide bridged dimer having slightly different Hg–P (2.437(7), 2.470(7) Å) bond distances and displays three AX resonances in its CP/MAS $^{31}P\{^1H\}$ NMR spectrum. Compound **4** is an unsymmetrical doubly iodide bridged dimer $[(Bu_3P)_2HgI_2HgI_2]$ having equivalent Hg–P (2.393(21), 2.391(22) Å) bond lengths but its CP/MAS $^{31}P\{^1H\}$ NMR spectrum shows two ABX resonances arising from the two different molecules in the unit cell with the phosphines being magnetically inequivalent in each molecule. Variable temperature ^{31}P NMR spectroscopy shows that equilibria between monomeric $(R_3P)_2HgX_2$ and dimeric $[R_3PHgX_2]_2$ occur in solution and for R_3P = DMPP and Bu_3P the dimers are very easily formed from the monomers.

Introduction

Mercury(II) halides HgX_2 (X = Cl, Br, I) form a wide variety of complexes L_nHgX_2 with tertiary phosphine ligands L [1–31]. The predominant stoichiometries are 1:1 and 2:1 ($n=1$, 2), although several examples of complexes with lower ligand to HgX_2 ratios have been reported [1]. The 2:1 complexes $[L_2HgX_2]$ have mononuclear pseudotetrahedral structures [4, 7, 11, 14]. The structural chemistry of the 1:1 complexes is more diverse, and dimers, [5, 8, 10, 12, 13, 15, 16] tetramers [5] and infinite chain polymers [6] have been characterized. The dimeric complexes $[L_2Hg_2X_4]$ can adopt symmetrical (**A**) or unsymmetrical (**B**) structures, depending on the nature of the ligand L.

---

*Authors to whom correspondence should be addressed.

**Present address: Chemagnetics, Inc., 2555 Midpoint Ave., Fort Collins, CO 80525, USA.

0020-1693/93/$6.00

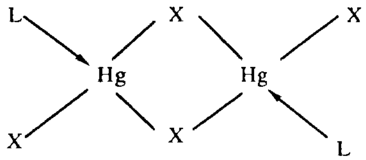

A

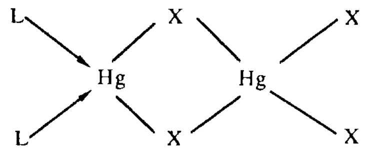

B

Of these, the most commonly observed is the symmetrical structure. The unsymmetrical structure occurs with ligands such as PPr_3 and PBu_3, and for $X = I$ [15, 23, 27]. With the more basic and sterically less demanding ligand, PMe_3 and PEt_3, chain polymer structures are observed [6].

Phospholes, such as 1-phenyl-3,4-dimethylphosphole (DMPP) [32–36] and 1-phenyl-dibenzophosphole (DBP) [37, 38], are phosphorus donor ligands with unusual donor properties. We have recently reported studies of the complexes of these two phosphole ligands with gold(I) [39] and gold(III) [40], copper(I) [41] and silver(I) [42] halides which showed that these ligands have significantly different coordination properties compared with those of PPh_3. As part of a continuing program of investigation of the structures and properties of transition metal phosphole complexes [33, 34, 37–47], we now report the results of a study of a number of mercury(II) complexes with the phospholes DMPP and DBP. No mercury(II) complexes of these ligands have previously been isolated, although the crystal structure of 1:1 complex of the closely related ligand 1,2,5-triphenylphosphole (TPP) with $HgCl_2$ has been reported [5].

The methods previously used to investigate the structure and bonding in phosphine/HgX_2 complexes are X-ray diffraction [4–16], vibrational spectroscopy [7–10, 12, 17–20] and NMR [20–31]. It has been possible to establish correlations between vibrational spectra and structure for complexes in the solid state, and structures for some have been proposed from their vibrational spectra alone. However, the range of possible structures is considerable, particularly for the 1:1 complexes, and some authors have emphasized the difficulties involved in drawing any definite structural conclusions from the vibrational spectra [10, 12]. NMR spectroscopy has been very useful in obtaining information about the nature of species in solution, but there have been relatively few studies of complexes in the solid state [48]. In one such study, the ^{31}P cross-polarization magic angle spinning (CP/MAS) NMR spectra of several 2:1 complexes of the type $[(PPh_3)_2HgX_2]$ ($X = Cl$, Br, I, SCN, CN) of known crystal structure were reported, and the results were discussed in terms of the structures [21]. No such studies of 1:1 complexes, which display a considerably greater range of structures, has yet been reported.

In order to further study the usefulness of these techniques for the investigation of structure and bonding, we have applied them to the series of new phosphole complexes prepared in the present study, and to a number of other phosphine/HgX_2 complexes of known and unknown structures. The structural conclusions reached in several cases have been checked by means of X-ray crystallography.

Experimental

Reagents and physical measurements

All chemicals were reagent grade and were used as received or synthesized as described below. When necessary, solvents were dried by standard procedures and stored over Linde 4-Å molecular sieves. All reactions involving phosphines or phospholes were conducted under an N_2 atmosphere. Mercury(II) chloride, bromide and iodide were purchased from J. T. Baker. 1-Phenyl-3,4-dimethylphosphole [49] (DMPP) and 1-phenyldibenzophosphole [43] (DBP) were prepared by literature methods.

Elemental analyses were performed by Galbraith Laboratories, Knoxville, TN. Melting points were determined on a Meltemp apparatus and are uncorrected.

IR spectra were recorded at 4 cm^{-1} resolution at room temperature as pressed KBr discs on a Digilab FTS-60 Fourier Transform infrared spectrometer employing an uncooled DTGS detector. Far-IR spectra were recorded at 4 cm^{-1} resolution at room temperature as pressed polythene discs on a Digilab FTS-60 Fourier Transform infrared spectrometer employing an FTS-60V vacuum optical bench with a 6.25 μm mylar film beam splitter, a mercury lamp source and a TGS detector. Raman spectra were excited with 100 mW of Ar^+ 514.5 nm radiation using a Coherent model 52 argon ion laser, and were recorded at 4.5 cm^{-1} resolution using a Jobin-Yvon U1000 spectrometer.

Solid state cross-polarization magic angle spinning (CP/MAS) $^{31}P\{^1H\}$ NMR spectra were obtained on a Nicolet NT-150 (^{31}P at 60.745 MHz) spectrometer using 20 kHz sweep widths, recycle delay times of 1–30 s, and proton decoupling fields of 10 mT. Between 200 and 300 mg of the compounds were spun at 3–4.5 kHz in Delrin or Kel-F rotors. The chemical shifts were referenced to 85% H_3PO_4 via an external sample of solid PPh_3 ($\delta = -6.0$ ppm). The uncertainties in chemical shifts and coupling constants are estimated to be ±0.5 ppm and ±10 Hz, respectively. The solution $^{31}P\{^1H\}$ NMR spectra were recorded at 40.26 MHz on a JEOL FX-100 and at 121.66 MHz on a General Electric GN-300 spectrometer on $CDCl_3/CH_2Cl_2$ (1:1) solutions. The chemical shifts were referenced to 85% H_3PO_4 via external PPh_3 ($\delta = -6.0$ ppm) with shifts to low field (high frequency) positive.

Syntheses

All preparations were carried out under an atmosphere of dry nitrogen. The $[L_nHgX_2]_m$ compounds ($L = PPh_3$ [5, 18, 20, 21, 25], PEt_3 [6, 12, 50, 51] and PBu_3 [5, 8, 23, 27]) were prepared according to literature procedures by reacting the appropriate mercury(II) halide with a slight excess of the phosphorus ligand (Strem Chemicals or Organometallics Inc.) in CH_2Cl_2, C_2H_5OH or C_6H_6.

L_2HgX_2 (L = DMPP, DBP)

To a suspension of about 3 g (approximately 10 mmol) of HgX_2 in 50 ml $CHCl_3$ under a nitrogen atmosphere was added 20 mmol of DMPP or DBP. After heating and stirring the mixture for about 1 h, pale yellow solutions were obtained. The solutions were filtered to remove any undissolved solids, the volumes of the filtrates were reduced to about 10 ml on a rotary evaporator, and hexane was added to induce crystallization. The products were isolated by filtration, washed with hexane and dried under vacuum. The DMPP complexes cannot be recrystallized as the complex dissociates DMPP forming $[(DMPP)HgX_2]_2$ as isolable solids.

$[LHgX_2]_2$ (L = DMPP, DBP)

To a solution containing about 1 g (approximately 3 mmol) of HgX_2 in 30 ml ethanol/dimethoxypropane (1:1) under a nitrogen atmosphere was added one molar equiv. of DMPP or DBP. The solution was heated at reflux for 0.5 h, cooled gradually to ambient temperature and left standing overnight. The precipitates that formed were isolated by filtration, washed with cold absolute ethanol and vacuum dried. The elemental analyses, melting points and yields of the complexes are given in Table 1.

Crystal structure analyses

Colorless crystals of $(DBP)_2HgBr_2$ (**1**), $[PPh_3HgBr_2]_2$ (**2**), pale yellow crystals of $[(DMPP)HgI_2]_2$ (**3**) and pale yellow crystals of $[(PBu_3)HgI_2]_2$ (**4**) were isolated from $CHCl_3/Et_2O$ solutions. Crystal data and additional details of data collection and refinement are given in Table 2. Intensity data for **1** and **2** were taken with a Rigaku AFC6S diffractometer in the ω–2θ mode, for **3** with a Siemens R3m diffractometer in the ω–2θ mode and for **4** with a Nicolet $P2_1$ diffractometer in the ω–2θ mode. The data were corrected for Lorentz, polarization and absorption effects. For **1** and **2** empirical absorption corrections were employed using the program DIFABS [52] and for **3** and **4** absorption corrections were made by the Gaussian method. Three standard reflections were monitored every 200 reflections and showed no changes during data collection for **1** and **2** but **3** showed a (50% on I) decrease and **4** showed a (6% on I) decrease and these data were rescaled to correct for this. Systematic absences ($h0l$, $h \neq 2n$, $0k0$, $k \neq 2n$) for **2**, ($0kl$, $k = 2n$, $h0l$, $l = 2n$) for **3** and ($h0l$, $l = 2n$, $0k0$, $k = 2n$) for **4** indicated space group $P2_1/a$ for **2**, $Pbc2_1$ or $Pbcm$ for **3** and $P2_1/c$ for **4**. No systematic absences were found for **1**. The structures of **1** and **2** were solved by direct methods. For **3** and **4** the heavy atoms were located by Patterson techniques, and the light atoms were then found on successive Fourier syntheses. The phenyl groups of **2** were refined as rigid hexagons with C–C = 1.40 Å. Anisotropic temperature factors were used for the Hg, Br and P atoms only. Anisotropic temperature factors were used for all non-hydrogen atoms for **1**, **3** and **4**. Except for **4**, hydrogen atoms were given fixed isotropic temperature factors, $U = 0.07$ Å^2 (**1**, **2**), 0.08 Å^2 (**3**), and were inserted at calculated positions and not refined. Final refinements were on F by least-squares methods. Weighting schemes of the form $1/(\sigma^2(F) + gF^2)$ were shown to be satisfactory by weight analyses. Computing was done with TEXAN [53] (**1**, **2**) or SHELXTL PLUS [54] (**3**, **4**) on Dec Microvax-II computers. Scattering factors were taken from ref. 55. Final atom coordinates are given in Tables 3–6, and selected bond lengths and angles in Tables 7–9. For **3** the crystals included a major yellow phase and a minor off-white component (not investigated further). For **4** the crystals were of two types, a main phase of very thin yellow plates, mixed with a few small lath-shaped colorless crystals. Crystals of the latter type were poorly ordered and gave weak diffuse X-ray peaks. They appeared to be orthorhombic, $a = 14.42(2)$, $b = 18.5(3)$, $c = 20.60(4)$ Å, $U = 5500$ Å^3; data were taken to $2\theta = 45°$, but the scattering was so weak that the space group could not be unambiguously assigned. No structure solution was possible, but the different unit cell volume suggests that this is not the same compound as the bulk material. For the main phase, data were collected for a small platy crystal; this also scattered weakly, but the crystals were of somewhat better quality than those of the other phase. Location and refinement of the butyl chains proved difficult and tedious. Weak constraints were used for all P–C (1.85(2) Å), C–C (1.51(4) Å) and non-bonded C–P–C (3.01(8) Å) distances. Several of the chains were disordered and some atoms were included in alternative positions with 0.5 occupancies. Most of the largest residual peaks were in the vicinity of these disordered chains. The refinement

TABLE 1. Elemental analyses, melting points and yields of new compounds

Compound	Calc. (found) (%)			Melting point (°C)	Yield (%)
	C	H	X		
$(DBP)_2HgCl_2$	54.61 (54.28)	3.28 (3.01)	8.95 (8.68)	260–262	76
$(DBP)_2HgBr_2$	49.09 (48.93)	2.95 (3.02)	18.15 (18.03)	245–246	82
$(DBP)_2HgI_2$	44.36 (44.25)	2.67 (2.51)	26.04 (25.87)	216–217	88
$[(DBP)HgCl_2]_2$	40.66 (40.73)	2.45 (2.34)	13.33 (13.06)	278–286	46
$[(DBP)HgBr_2]_2$	34.83 (34.65)	2.09 (2.18)	25.75 (25.29)	264–270	92
$[(DBP)HgI_2]_2$	30.26 (30.15)	1.82 (2.16)	35.52 (35.36)	218–222	88
$(DMPP)_2HgCl_2$	44.51 (44.34)	4.01 (4.29)	10.95 (10.53)	174–175	81
$(DMPP)_2HgBr_2$	39.13 (39.21)	3.53 (3.36)	21.70 (21.91)	170–172	75
$(DMPP)_2HgI_2$	34.71 (34.53)	3.13 (3.20)	30.56 (30.38)	176–180	73
$[(DMPP)HgCl_2]_2$	31.36 (31.31)	2.83 (2.86)	15.43 (15.02)	199–202	88
$[(DMPP)HgBr_2]_2$	26.28 (26.31)	2.37 (2.18)	29.14 (29.22)	166–168	87
$[(DMPP)HgI_2]_2$	22.43 (22.36)	2.02 (1.97)	39.50 (39.34)	144–152	82

TABLE 2. Crystallographic data for compounds **1**–**4**

Compound	$[(DBP)_2HgBr_2]$ (**1**)	$[(PPh_3)HgBr_2]_2$ (**2**)	$[(DMPP)HgI_2]_2$ (**3**)	$[(Bu_3P)HgI_2]_2$ (**4**)
Chemical formula	$C_{36}H_{26}Br_2HgP_2$	$C_{36}H_{30}Br_4Hg_2P_2$	$C_{24}H_{26}Hg_2I_4P_2$	$C_{24}H_{54}Hg_2I_4P_2$
Formula weight	880.95	1245.38	1285.2	1313.4
a (Å)	10.568(6)	18.619(7)	8.516(4)	16.450(16)
b (Å)	17.390(6)	10.938(4)	19.404(7)	20.609(21)
c (Å)	9.610(3)	18.762(5)	19.545(6)	24.263(31)
α (°)	106.02(4)	90	90	90
β (°)	100.62(4)	90.36(2)	90	109.38(8)
γ (°)	101.41(5)	90	90	90
V (Å^3)	1610(1)	3821(2)	3230(2)	7560
Z	2	4	4	8
Space group	$P\bar{1}$	$P2_1/a$	$Pbc2_1$	$P2_1/c$
T (°C)	25	25	17	17
λ (Å)	0.71069	0.71069	0.71069	0.71069
ρ_{calc} (g cm^{-3})	1.817	2.165	2.64	2.31
μ (cm^{-1})	73.6	122.8	13.4	111.5
Transmission factor range	0.55–1.00	0.89–1.10	0.11–0.24	
$R(F)^a$	0.042	0.070	0.040	0.067
$R_w(F)^b$	0.029	0.067	0.047	0.075

$^aR(F)=\Sigma w(|F_o|-|F_c|)^2$ with $\sigma^2(F)^2=\sigma^2$ (counts) $+(pI)^2$. $^bR_w(F)=\Sigma w[(|F_o|-|F_c|^2)/\Sigma w|F_o|^2]^{1/2}$.

difficulty, the relatively large residual peaks and the high final R value are easily understandable in the light of the weak scattering and highly anisotropic absorption. Anisotropic temperature factors were used for Hg, I and P atoms. Hydrogen atoms were omitted.

Results and discussion

The phosphole ligands 1-phenyl-3,4-dimethylphosphole (DMPP) and 1-phenyldibenzophosphole (DBP) were reacted with the mercury(II) halides HgX_2 (X = Cl, Br, I) in mole ratios of 1:1 and 2:1. Complexes of 1:1 and 2:1 stoichiometry were obtained in all cases, although the 2:1 complex of DMPP with $HgCl_2$ is very unstable, and readily dissociates DMPP to form the 1:1 complex. This behaviour contrasts with that of PPh_3 and PEt_3, both of which form a complete set of 1:1 and 2:1 complexes with the mercury(II) halides. The trend noted above for the 2:1 DMPP complexes (the chloride being the least stable) is exactly the reverse of that found for the PBu_3 complexes where we could obtain the 2:1 complex only for the chloride (but see refs. 23 and 50). Clearly there are differences in the ways that these ligands bind to the mercury atom which have significant effects on the relative stabilities of the different complexes that they can form. Structural and spectroscopic studies help to shed further light on the reasons for these differences.

Crystal structures of $[(DBP)_2HgBr_2]$, $[(PPh_3)_2Hg_2Br_4]$, $[(DMPP)_2Hg_2I_4]$ and $[(Bu_3P)_2Hg_2I_4]$

The crystal structure of the 2:1 complex $[(DBP)_2HgBr_2]$ (**1**) reveals that this species is mono-

TABLE 3. Atom coordinates for $(DBP)_2HgBr_2$ (1)[a]

Atom	x	y	z	B_{eq}
Hg(1)	1.14070(5)	0.25982(3)	1.08705(5)	3.18(2)
Br(1)	1.0961(1)	0.14574(9)	1.2149(1)	5.74(6)
Br(2)	1.2513(1)	0.40135(8)	1.2986(1)	5.77(6)
P(1)	1.3211(3)	0.2165(2)	0.9718(3)	3.0(1)
P(2)	0.9320(3)	0.2640(2)	0.9230(3)	3.0(1)
C(1)	1.459(1)	0.2055(7)	1.102(1)	3.3(5)
C(2)	1.498(1)	0.2591(8)	1.247(1)	4.4(5)
C(3)	1.603(1)	0.2519(9)	1.352(1)	5.5(6)
C(4)	1.667(1)	0.190(1)	1.310(1)	4.9(6)
C(5)	1.627(1)	0.1378(8)	1.166(1)	5.0(6)
C(6)	1.523(1)	0.1437(8)	1.059(1)	4.5(5)
C(7)	1.383(1)	0.2763(8)	0.860(1)	3.1(5)
C(8)	1.452(1)	0.3605(8)	0.910(1)	3.9(5)
C(9)	1.479(1)	0.3957(7)	0.803(1)	4.1(5)
C(10)	1.439(1)	0.3529(9)	0.653(1)	4.3(6)
C(11)	1.368(1)	0.2687(8)	0.604(1)	3.8(5)
C(12)	1.342(1)	0.2303(7)	0.710(1)	2.5(4)
C(13)	1.271(1)	0.1418(8)	0.681(1)	3.1(5)
C(14)	1.256(1)	0.1230(7)	0.811(1)	2.9(4)
C(15)	1.196(1)	0.0454(8)	0.805(1)	3.8(5)
C(16)	1.151(1)	−0.0182(7)	0.667(1)	4.3(5)
C(17)	1.164(1)	−0.0002(7)	0.540(1)	4.0(5)
C(18)	1.225(1)	0.0807(8)	0.545(1)	3.6(5)
C(19)	0.799(1)	0.1672(7)	0.838(1)	3.3(5)
C(20)	0.682(1)	0.1675(8)	0.745(1)	4.4(5)
C(21)	0.581(1)	0.095(1)	0.682(1)	4.9(6)
C(22)	0.593(1)	0.0249(9)	0.713(1)	5.3(6)
C(23)	0.708(1)	0.0231(8)	0.806(1)	5.0(6)
C(24)	0.811(1)	0.0955(8)	0.870(1)	3.8(5)
C(25)	0.861(1)	0.3460(6)	1.008(1)	2.7(4)
C(26)	0.820(1)	0.3576(8)	1.135(1)	4.3(6)
C(27)	0.775(1)	0.4287(9)	1.186(1)	4.8(6)
C(28)	0.776(1)	0.4854(8)	1.109(2)	4.6(6)
C(29)	0.815(1)	0.4705(7)	0.977(1)	3.9(5)
C(30)	0.858(1)	0.4003(7)	0.924(1)	2.7(4)
C(31)	0.909(1)	0.3762(7)	0.789(1)	2.9(4)
C(32)	0.914(1)	0.4157(7)	0.682(1)	4.2(5)
C(33)	0.969(1)	0.3847(9)	0.566(1)	5.2(6)
C(34)	1.017(1)	0.3149(9)	0.551(1)	4.9(6)
C(35)	1.011(1)	0.2744(7)	0.656(1)	3.6(5)
C(36)	0.955(1)	0.3038(7)	0.771(1)	2.9(4)

[a] Anisotropically refined atoms are given in the form of the isotropic equivalent displacement parameter defined as: $(4/3)[a^2\beta(1,1)+b^2\beta(2,2)+c^2\beta(3,3)+ab(\cos\gamma)\beta(1,2)+ac(\cos\beta)\text{-}\beta(1,3)+bc(\cos\alpha)\beta(2,3)]$.

TABLE 4. Atom coordinates for $[(PPh_3)HgBr_2]_2$ (2)[a]

Atom	x	y	z	B_{eq}
Hg(1)	0.3357(1)	0.1377(2)	0.1755(1)	3.9(2)
Hg(2)	0.1820(1)	0.0705(2)	0.3098(1)	4.0(2)
Br(1)	0.4431(3)	0.0074(7)	0.2011(4)	5.5(4)
Br(2)	0.0709(3)	0.1933(7)	0.2859(3)	5.3(4)
Br(3)	0.2920(3)	0.2317(6)	0.3079(3)	4.4(4)
Br(4)	0.2246(3)	−0.0238(6)	0.1786(3)	4.4(4)
P(1)	0.3140(7)	0.309(1)	0.0987(8)	3.0(9)
P(2)	0.2035(8)	−0.094(1)	0.3952(7)	3.1(9)
C(1)	0.368(2)	0.301(4)	0.020(1)	4.6(7)
C(2)	0.373(2)	0.191(3)	−0.017(2)	4.6(7)
C(3)	0.412(2)	0.184(3)	−0.080(2)	4.6(7)
C(4)	0.446(2)	0.287(4)	−0.107(1)	4.6(7)
C(5)	0.441(2)	0.398(3)	−0.070(2)	4.6(7)
C(6)	0.402(2)	0.405(3)	−0.007(2)	4.6(7)
C(7)	0.335(2)	0.452(3)	0.146(2)	3.0(5)
C(8)	0.399(2)	0.450(2)	0.185(2)	3.0(5)
C(9)	0.422(1)	0.555(3)	0.221(1)	3.0(5)
C(10)	0.381(2)	0.662(2)	0.218(1)	3.0(5)
C(11)	0.317(2)	0.664(2)	0.179(2)	3.0(5)
C(12)	0.294(1)	0.559(3)	0.143(1)	3.0(5)
C(13)	0.221(1)	0.318(3)	0.073(2)	4.8(7)
C(14)	0.203(2)	0.338(3)	0.002(2)	4.8(7)
C(15)	0.132(2)	0.345(3)	−0.019(1)	4.8(7)
C(16)	0.077(1)	0.332(3)	0.031(2)	4.8(7)
C(17)	0.095(2)	0.312(3)	0.103(2)	4.8(7)
C(18)	0.167(2)	0.305(3)	0.124(1)	4.8(7)
C(19)	0.293(1)	−0.094(3)	0.430(2)	4.1(6)
C(20)	0.349(2)	−0.075(3)	0.382(1)	4.1(6)
C(21)	0.420(2)	−0.082(3)	0.406(2)	4.1(6)
C(22)	0.435(1)	−0.107(3)	0.477(2)	4.1(6)
C(23)	0.380(2)	−0.125(3)	0.525(1)	4.1(6)
C(24)	0.308(2)	−0.119(3)	0.502(2)	4.1(6)
C(25)	0.187(2)	−0.234(3)	0.354(2)	5.4(7)
C(26)	0.240(2)	−0.324(4)	0.360(2)	5.4(7)
C(27)	0.227(2)	−0.441(3)	0.333(2)	5.4(7)
C(28)	0.161(2)	−0.468(3)	0.300(2)	5.4(7)
C(29)	0.109(2)	−0.378(4)	0.294(2)	5.4(7)
C(30)	0.122(2)	−0.261(3)	0.321(2)	5.4(7)
C(31)	0.145(1)	−0.084(4)	0.472(1)	4.1(6)
C(32)	0.126(2)	0.033(3)	0.495(2)	4.1(6)
C(33)	0.083(2)	0.047(3)	0.554(2)	4.1(6)
C(34)	0.057(1)	−0.055(4)	0.591(1)	4.1(6)
C(35)	0.076(2)	−0.172(3)	0.567(2)	4.1(6)
C(36)	0.120(2)	−0.186(3)	0.508(2)	4.1(6)

[a] Anisotropically refined atoms are given in the form of the isotropic equivalent displacement parameter defined as: $(4/3)[a^2\beta(1,1)+b^2\beta(2,2)+c^2\beta(3,3)+ab(\cos\gamma)\beta(1,2)+ac(\cos\beta)\text{-}\beta(1,3)+bc(\cos)\beta(2,3)]$.

nuclear with pseudotetrahedral coordination at the mercury atom. The structure is similar to those previously reported for $[(PPh_3)_2HgX_2]$ (X = Cl, Br, I) [4, 11]. Selected structural parameters for $[L_2HgBr_2]$ (L = DBP, PPh_3) are compared in Table 7, and the structure of the DBP complex is shown in Fig. 1. It is clear that the structures of the DBP and PPh_3 complexes are quite similar, but a noticeable difference is that *both* the Hg–P *and* the Hg–Br bond lengths are shorter in the case of the DBP complex. The P–Hg–P angle is significantly larger in the DBP complex, but the Br–Hg–Br angles are almost equal in the two complexes.

The crystal structures of the 1:1 complexes $[(PPh_3)_2Hg_2Br_4]$ (**2**) and $[(DMPP)_2Hg_2I_4]$ (**3**) show the symmetric dimer structure **A** above, similar to the previously determined structures of $[(PPh_3)_2Hg_2X_4]$ (X = Cl, I) [5, 16]. However, whereas the X = Cl compound has a perfectly centrosymmetric structure, the X = Br, I complexes have non-centrosymmetric struc-

TABLE 5. Atom coordinates (×10^4) for [(DMPP)HgI$_2$]$_2$ (3)[a]

Atom	x	y	z	U (Å^2×10^3)
Hg(1)	855.9(14)	1189.4(5)	5000.0	62(1)*
Hg(2)	2134.7(14)	1265.3(5)	3114.4(8)	66(1)*
I(1)	410.3(25)	2262.2(8)	3942.4(10)	65(1)*
I(2)	2540.8(26)	153.9(8)	4123.9(11)	65(1)*
I(3)	4886.4(28)	1764.9(11)	2731.9(13)	79(1)*
I(4)	−1938.7(24)	692.4(9)	5297.9(12)	64(1)*
P(1)	3158(8)	1702(3)	5539(4)	51(2)*
P(2)	−36(9)	750(3)	2451(3)	49(2)*
C(11)	4025(31)	1158(10)	6187(11)	43(8)*
C(12)	4949(35)	1462(16)	6708(16)	70(11)*
C(13)	5530(39)	1010(23)	7189(18)	100(18)*
C(14)	5271(42)	342(18)	7175(17)	80(13)*
C(15)	4388(33)	70(13)	6673(14)	54(9)*
C(16)	3702(38)	470(12)	6217(12)	61(10)*
C(17)	4484(32)	1959(13)	4902(13)	58(10)*
C(18)	4612(30)	2653(13)	4858(12)	52(9)*
C(19)	5508(45)	3048(15)	4338(18)	90(14)*
C(110)	3652(38)	3007(15)	5445(16)	76(12)*
C(111)	3594(46)	3755(14)	5509(18)	82(13)*
C(112)	2862(31)	2560(14)	5812(13)	57(9)*
C(21)	−707(30)	1284(11)	1746(12)	42(8)*
C(22)	−723(41)	1025(11)	1116(14)	79(12)*
C(23)	−1096(45)	1455(14)	558(14)	83(13)*
C(24)	−1604(38)	2150(13)	683(13)	67(11)*
C(25)	−1631(36)	2371(14)	1336(14)	66(11)*
C(26)	−1149(32)	1959(15)	1873(15)	66(11)*
C(27)	−1454(37)	482(13)	3008(12)	62(10)*
C(28)	−1439(33)	−207(13)	3053(13)	54(9)*
C(29)	−2420(43)	−602(20)	3552(18)	96(15)*
C(210)	−474(34)	−521(12)	2550(14)	55(9)*
C(211)	−414(54)	−1314(13)	2468(24)	112(18)*
C(212)	366(36)	−92(13)	2157(12)	56(10)*

[a] Equivalent isotropic U defined as one third of the trace of the orthogonalized U_{ij} tensor.

TABLE 6. Atom coordinates (×10^4) for [(Bu$_3$P)HgI$_2$]$_2$ (**4**)[a]

Atom	x	y	z	U (Å^2×10^3)
Hg(11)	741.0(16)	3835.2(12)	2182.2(11)	72(1)*
I(11)	1574(3)	4997(2)	3095(2)	79(2)*
I(12)	1876(3)	2898(2)	3066(2)	77(2)*
Hg(12)	2567.9(17)	4006.1(13)	3802.1(12)	84(1)*
I(13)	4220(3)	4055(2)	3811(2)	106(2)*
I(14)	2250(3)	3935(2)	4810(2)	116(3)*
P(11)	−466(11)	3758(8)	2520(8)	85(9)*
P(12)	1614(12)	4070(9)	1592(8)	95(10)*
C(111)	−130(32)	3715(24)	3323(11)	81(19)
C(112)	−815(34)	3650(28)	3614(23)	102(22)
C(113)	−438(36)	3521(28)	4272(23)	91(21)
C(114)	46(47)	2886(32)	4364(34)	164(32)
C(121)	−1199(35)	3058(21)	2253(26)	134(28)
C(122)	−713(44)	2433(32)	2426(34)	156(32)
C(123)	−1451(47)	1953(34)	2156(31)	141(30)
C(124)	−2232(48)	1859(37)	2346(33)	159(32)
C(131)	−1272(51)	4496(30)	2285(32)	187(38)
C(132)$^{+}$	−815(59)	5107(41)	2266(52)	87(42)
C(13b)$^{+}$	−1104(77)	4850(49)	1802(44)	94(43)
C(133)$^{+}$	−1668(64)	5397(50)	1870(54)	58(50)
C(13c)$^{+}$	−1788(105)	5652(90)	1822(77)	134(78)
C(134)	−1242(74)	5982(51)	2226(48)	96(45)
C(141)	1792(33)	3371(17)	1162(18)	76(19)
C(142)$^{+}$	1649(95)	2717(32)	1387(70)	167(75)
C(14b)$^{+}$	2163(55)	2827(28)	1567(26)	19(25)
C(143)	2188(45)	2226(31)	1203(28)	119(26)
C(144)	2439(57)	1586(37)	1513(37)	197(40)
C(151)	2680(22)	4315(24)	2103(20)	83(20)
C(152)	3274(43)	4449(34)	1751(28)	138(29)
C(153)	4072(47)	4835(34)	2131(33)	162(33)
C(154)	3952(49)	5509(34)	2324(33)	149(30)
C(161)	1165(35)	4687(20)	1009(18)	91(22)
C(162)$^{+}$	861(50)	5210(33)	1321(31)	10(23)
C(16b)$^{+}$	256(82)	4978(108)	862(104)	278(124)
C(163)$^{+}$	541(125)	5413(88)	682(51)	174(96)
C(16c)$^{+}$	819(168)	5608(100)	1203(75)	385(146)
C(164)	36(62)	5991(46)	759(42)	192(39)
Hg(21)	−3972.2(16)	2744.7(12)	4554.1(11)	76(1)*
I(21)	−2636(3)	2052(2)	4099(2)	87(2)*
I(22)	−3314(3)	1996(2)	5708(2)	84(2)*
Hg(22)	−2186.0(18)	1381.5(14)	5182.9(12)	100(2)*
I(23)	−594(3)	1829(3)	5816(2)	119(3)*
I(24)	−2529(4)	123(3)	5065(3)	143(4)*
P(21)	−3159(11)	3710(8)	4949(7)	84(9)*
P(22)	−5134(12)	2058(8)	4036(8)	91(9)*
C(211)	−2007(17)	3504(24)	5280(22)	91(21)
C(212)	−1497(32)	4135(24)	5415(24)	88(21)
C(213)	−576(32)	3920(26)	5791(23)	80(19)
C(214)	58(40)	4461(30)	5814(29)	123(26)
C(221)	−3367(39)	4384(23)	4427(22)	117(25)
C(222)	−3089(51)	4147(36)	3912(32)	158(32)
C(223)$^{+}$	−3275(81)	4836(41)	3669(52)	94(43)
C(22c)$^{+}$	−3170(92)	4309(54)	3283(38)	125(54)
C(224)$^{+}$	−2899(119)	4900(90)	3183(67)	177(77)
C(22d)$^{+}$	−3620(74)	4938(50)	3081(48)	72(39)
C(231)	−3498(44)	3916(36)	5616(28)	159(32)
C(232)	−4448(48)	3903(54)	5454(44)	258(53)
C(233)	−4342(63)	3905(53)	6087(45)	226(46)
C(234)$^{+}$	−5312(66)	3868(89)	5940(75)	161(74)
C(23d)$^{+}$	−5041(96)	3481(74)	6178(71)	146(67)

(*continued*)

tures in which all of the Hg–P and Hg–I bond lengths are different. Selected structural parameters for [(PPh$_3$)$_2$Hg$_2$X$_4$] (X = Br,I) and [(DMPP)$_2$Hg$_2$I$_4$] are compared in Table 8 and the structures of [(PPh$_3$)$_2$Hg$_2$Br$_4$] and [(DMPP)$_2$Hg$_2$I$_4$] are shown in Figs. 2 and 3, respectively. In both structures each of the two mercury atoms is tetra-coordinated, forming bonds with the P atom of one ligand, a terminal halide atom and the two doubly bridging halide atoms. Each molecule has two different phoshorus environments P(1) and P(2). Some systematic differences are observed among the various structures. First, the Hg–P bond lengths in [(PPh$_3$)$_2$Hg$_2$X$_4$] increase monotomically from (X = Cl to I), corresponding to a decrease in the acceptor strength of the mercury halide along this series. There is an increase in the bridging X$_b$–Hg–X$_b$ angle and a corresponding decrease in the bridging Hg–X$_b$–Hg angle from X = Cl to I, as is often observed in structures involving doubly bridging halogen atoms. Comparing [(PPh$_3$)$_2$Hg$_2$I$_4$] and [(DMPP)$_2$Hg$_2$I$_4$], it is again observed that both the Hg–P and the terminal Hg–I$_t$ bond lengths

TABLE 6. (*continued*)

Atom	x	y	z	U (Å^2×10^3)
C(241)	−6101(23)	2191(24)	4259(21)	71(18)
C(242)	−6029(54)	1882(39)	4827(28)	183(36)
C(243)	−6650(54)	1977(42)	5144(36)	178(36)
C(244)	−7503(61)	1731(54)	4754(44)	260(54)
C(251)	−5574(33)	2187(24)	3235(11)	80(19)
C(252)$^+$	−4794(61)	2202(70)	3035(56)	115(59)
C(25b)$^+$	−5027(70)	2606(53)	2984(48)	63(40)
C(253)$^+$	−5145(109)	2522(76)	2441(56)	106(57)
C(25c)$^+$	−5503(113)	2843(110)	2371(59)	187(119)
C(254)$^+$	−4374(106)	2804(96)	2307(88)	173(87)
C(25d)$^+$	−4797(129)	2879(92)	2100(79)	147(75)
C(261)	−4761(32)	1208(14)	4149(23)	97(22)
C(262)	−5464(35)	704(26)	3871(25)	96(22)
C(263)	−5251(43)	−7(29)	4074(29)	122(26)
C(264)	−5992(50)	−424(38)	3713(35)	183(36)

[a] Starred items: equivalent isotropic U defined as one third of the trace of the orthogonalized U_{ij} tensor. +0.5 occupancy.

TABLE 7. Core geometries for $[(PPh_3)_2HgBr_2]$ and $[(DBP_2HgBr_2]$

Parameter	$[(PPh_3)_2HgBr_2]$[a]	$[(DBP)_2HgBr_2]$
Hg–P(1)	2.535(15)	2.513(3)
Hg–P(2)	2.540(16)	2.490(3)
Hg–Br(1)	2.633(6)	2.618(2)
Hg–Br(2)	2.626(8)	2.604(2)
P(1)–Hg–P(2)	113.0(5)	119.4(1)
Br(1)–Hg–Br(2)	106.9(3)	107.56(6)

[a] Ref. 11.

are slightly smaller in the phosphole complex (cf. similar behaviour in $[(DBP)_2HgBr_2]$ compared with $[(PPh_3)_2HgBr_2]$ discussed above). The most striking difference between the structures of these two complexes is the considerable increase in the P–Hg–I$_t$ angle from the PPh_3 to the DMPP complex. Both of the above observations indicate stronger Hg–P and Hg–I$_t$ bonding in the phosphole complex. This occurs at the expense of Hg–I$_b$ bonding, as shown by the longer Hg–I$_b$ bonds.

The compound $[(Bu_3P)_2Hg_2I_4]$ (**4**) shows the unsymmetrical dimer structure **B**, similar to that previously determined for the corresponding PPr_3 complex [14]. Selected structural parameters for these two complexes are compared in Table 9, and the structure of $[(Bu_3P)_2Hg_2I_4]$ is shown in Fig. 4. In this structure each of the two mercury atoms is tetra-coordinated; one by forming bonds with the P atoms of the two phosphine ligands and the two bridging iodine atoms, and the other by bonding to two terminal iodine atoms and the two bridging iodine atoms. Each molecule has two different phosphorus environments P(1) and P(2). The PBu_3 complex shows shorter Hg–P bond lengths and a greater P–Hg–P angle than the PPr_3 complex, which suggests that the P–Hg–P bonding is stronger in the PBu_3 case. These complexes can be regarded as $[L_2Hg]^{2+}$ and $[HgI_4]^{2-}$ species which are associated via Hg–I–Hg bonds involving two of the four I atoms in the second species, and the above results suggest that the structure more nearly approaches a description in terms of separate entities of this type for the PBu_3 case. In agreement with this, the average of the bridging bond lengths Hg(1)–I(1), Hg(1)–I(2) is greater, and the range of Hg(2)–I(x) (x = 1–4) is slightly less for the PBu_3 complex.

Far-infrared and Raman spectra

The wavenumbers of the bands in the far-IR and Raman spectra which have been assigned to Hg–X and

TABLE 8. Core geometries for $[(PPh_3)_2Hg_2Br_4]$, $[(PPh_3)_2Hg_2I_4]$ and $[(DMPP)_2Hg_2I_4]$

Parameter	$[(PPh_3)_2Hg_2Br_4]$	$[(PPh_3)_2Hg_2I_4]$[a]	$[(DMPP)_2Hg_2I_4]$[b]
Hg(1)–P(1)	2.40(2)	2.461(8)	2.437(7)
Hg(2)–P(2)	2.44(2)	2.483(8)	2.470(7)
Hg(1)–X(1)	2.499(7)	2.671(2)	2.633(3)
Hg(2)–X(2)	2.505(7)	2.684(2)	2.644(3)
Hg(1)–X(3)	2.813(7)	2.860(2)	2.958(2)
Hg(1)–X(4)	2.721(7)	2.990(2)	3.005(3)
Hg(2)–X(3)	2.704(7)	2.960(2)	2.918(3)
Hg(2)–X(4)	2.789(7)	2.846(2)	2.943(3)
P(1)–Hg(1)–X(1)	133.9(4)	128.4(2)	141.3(2)
P(2)–Hg(2)–X(2)	130.1(4)	126.6(2)	131.6(2)
X(3)–Hg(1)–X(4)	89.7(2)	94.8(1)	97.7(1)
X(3)–Hg(2)–X(4)	90.6(2)	95.8(1)	100.0(1)
Hg(1)–X(3)–Hg(2)	89.8(2)	84.9(1)	81.8(1)
Hg(1)–X(4)–Hg(2)	90.0(2)	84.6(1)	80.6(1)

[a] Ref. 16. [b] The atom numbering system used in the solution of the structure of $[(DMPP)_2Hg_2I_4]$ differs from that for the two PPh_3 complexes above. In order to facilitate comparison, the numbering system for the former complex has been changed to that of the latter two in the above Table. This involves the following transformations relative to the numbering system in Table 5: $I_1 \rightarrow I_3$; $I_2 \rightarrow I_4$; $I_3 \rightarrow I_2$; $I_4 \rightarrow I_1$.

TABLE 9. Core geometries for $[(Pr_3P)_2Hg_2I_4]$ and $[(Bu_3P)_2Hg_2I_4]$

Parameter	$[(Pr_3P)_2Hg_2I_4]^a$	$[(Bu_3P)_2Hg_2I_4]$	
		Molecule (1)	Molecule (2)
Hg(1)–P(1)	2.457(14)	2.393(1)	2.410(17)
Hg(1)–P(2)	2.421(15)	2.391(22)	2.375(17)
Hg(1)–I(1)	3.027(4)	3.240(6)	3.113(7)
Hg(1)–I(2)	3.050(5)	3.027(6)	3.063(6)
Hg(2)–I(1)	2.921(4)	2.816(6)	2.843(6)
Hg(2)–I(2)	2.937(5)	2.890(6)	2.871(6)
Hg(2)–I(3)	2.694(4)	2.713(7)	2.720(6)
Hg(2)–I(4)	2.685(5)	2.670(7)	2.650(7)
P(1)–Hg(1)–P(2)	149.1(5)	162.0(6)	160.9(6)
I(1)–Hg(1)–I(2)		88.1(1)	90.9(2)
Hg(1)–I(1)–Hg(2)		84.8(1)	83.9(2)
Hg(1)–I(2)–Hg(2)		87.5(1)	84.3(2)
I(1)–Hg(2)–I(2)		99.6(1)	100.8(2)
I(3)–Hg(2)–I(4)		119.7(2)	121.6(2)

[a]Ref. 15.

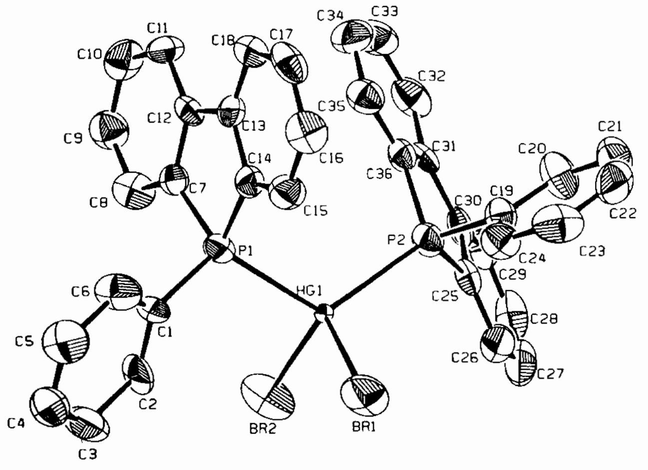

Fig. 1. ORTEP plot of the structure $(DBP)_2HgBr_2$ (**1**) showing the atom labelling scheme; thermal ellipsoids scaled to enclose 50% of the electron density. Hydrogen atoms omitted for clarity.

Hg–P modes, ν(HgX) and ν(HgP), are listed in Tables 10 and 11 for the 2:1 and 1:1 complexes, respectively. Data for the PPh_3 complexes have been reported previously, and the results obtained in the present study are in reasonable agreement with these. The results for the 2:1 complexes are discussed first, since these are simpler structurally, and more complete assignments of the vibrational bands are possible in this case.

2:1 Complexes

The complexes $[(DBP)_2HgX_2]$ show ν(HgX) and ν(HgP) bands at wavenumbers which are slightly higher than those of the corresponding PPh_3 compounds. In the case of the X = Br complex, this correlates well with the observation that both the Hg–X and the Hg–P bond lengths are shorter in the DBP complex (*vide supra*). The complexes $[(DMPP)_2HgX_2]$ show ν(HgX) bands at almost the same wavenumbers as their DBP counterparts. The X = Cl complex is particularly unstable and it was not possible to obtain a Raman spectrum because the sample decomposed in the laser

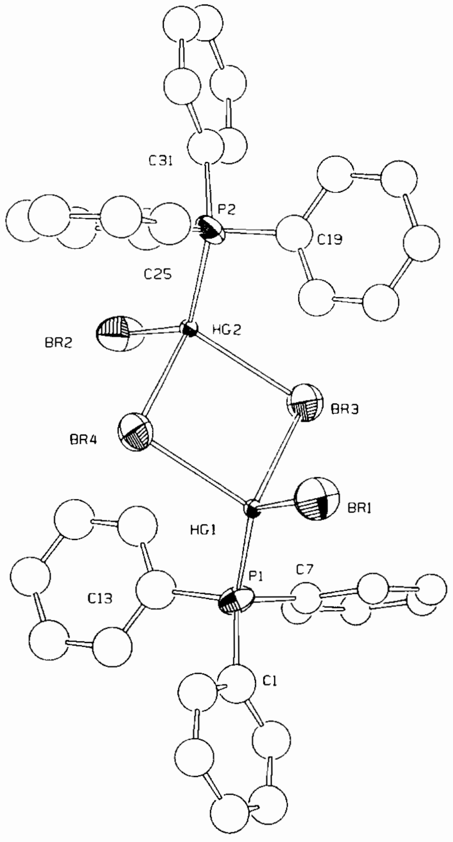

Fig. 2. ORTEP plot of the structure of $[(PPh_3)HgBr_2]_2$ (**2**) showing the atom labelling scheme; thermal ellipsoids scaled to enclose 50% of the electron density. Hydrogen atoms omitted for clarity.

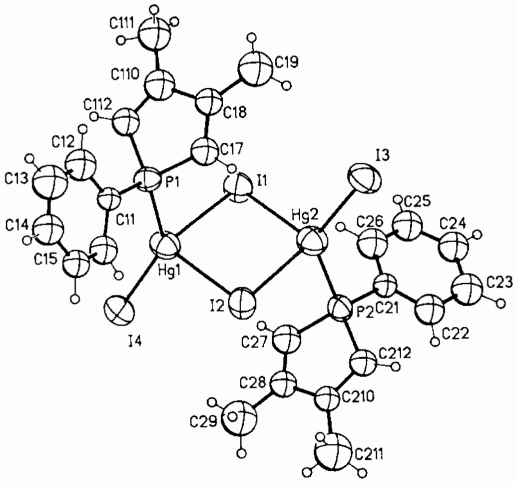

Fig. 3. ORTEP plot of the structure of $[(DMPP)HgI_2]_2$ (**3**) showing the atom labelling scheme; thermal ellipsoids scaled to enclose 50% of the electron density. Hydrogen atoms have an arbitrary radius of 0.1 Å.

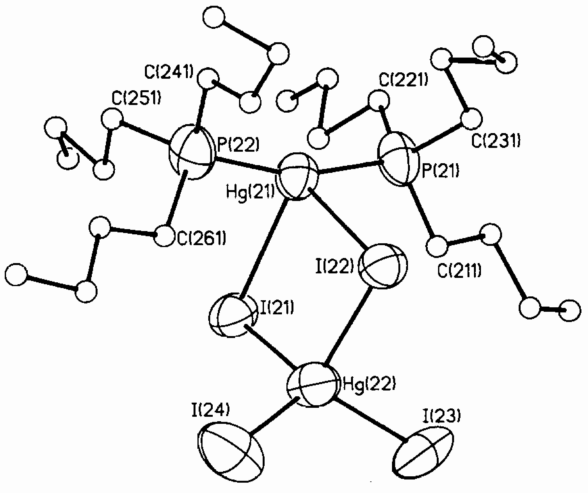

Fig. 4. ORTEP plot of the structure of $[(PBu_3)HgI_2]_2$ (4) showing the atom labelling scheme; thermal ellipsoids scaled to enclose 50% of the electron density. Carbon atoms have an arbitrary radius of 0.1 Å. Hydrogen atoms omitted for clarity.

TABLE 10. Metal–ligand vibrational frequencies (cm^{-1}) for $[L_2HgX_2]$

L	X	Method	$\nu(HgX_t)$	$\nu(HgP)$
PPh_3	Cl	IR	232, 221	137
		R	233, 214	133
	Br	IR	153	132
		R	157	135
	I	IR	127	133
		R	126	134
DBP	Cl	IR	246, 231	135
		R	245	138
	Br	IR	161	135
		R	164	137
	I	IR	132	139
		R	131	140
DMPP	Cl	IR	228	134
		R	(decomposes)	
	Br	IR	161	137
		R	162	137
	I	IR	130	130
		R	133	133
PEt_3	Cl	IR	183	
		R	193	151
	Br	IR	133	
		R		150
	I	IR	106	
		R	106	142
PBu_3	Cl	IR	205	
		R	211	128

TABLE 11. Metal–ligand vibrational frequencies (cm^{-1}) for $[LHgX_2]_2$

L	X	Method	$\nu(HgX_t)$	$\nu(HgX_b)$	$\nu(HgP)$
PPh_3	Cl	IR	291, 288	188, 183	157
		R	286		156
	Br	IR	203, 190	137, 117	
		R	200, 192	150	
	I	IR	163, 139	117, 89	
		R	160, 143	125	
DBP	Cl	IR	278, 270	224, 212	
		R	274	222	
	Br	IR	188	157, 139	
		R	184	159, 137	
	I	IR	153	139, 132	
		R	153	129	
DMPP	Cl	IR	273	210	
		R	269	206	
	Br	IR	189	145	
		R	186	154, 136	
	I	IR	175, 168	144	
		R	172	144	
PEt_3	Cl	IR	279	202	
		R	270, 264	214	
	Br	IR	188	149, 141	
		R	186	142	
	I	IR	145	90	
		R	140	112	
PBu_3	Cl (α-form)	IR	280	152	
		R	275	165	
	Cl (β-form)	IR	340, 309	185, 168	
		R	306	185, 168	
	Br	IR	188, 167	141, 122	
		R	186, 168	148	
	I	IR	150, 130		
		R	148, 128	113	

beam. However, there is no indication from the $\nu(HgCl)$ value in the IR that this compound should behave any differently from the others. For the X = I compounds $\nu(HgX)$ and $\nu(HgP)$ occur at essentially the same frequency, and in the DMPP case only a single band due to these modes is observed in each of the IR and Raman spectra.

The far-IR and Raman spectra of $[(PEt_3)_2HgX_2]$ are shown in Figs. 5 and 6. The assignments of the $\nu(HgX)$ and $\nu(HgP)$ bands follow along similar lines to those for the PPh_3 and the phoshole complexes. In this case, however, the $\nu(HgX)$ wavenumbers are lower and the $\nu(HgP)$ wavenumbers higher than in the corresponding PPh_3 and phosphole complexes, so that $\nu(HgP)$ becomes greater than $\nu(HgX)$ at X = Br, rather than X = I. These results suggest that the Hg–P bonding is much stronger, and the Hg–X bonding is correspondingly weaker in the PEt_3 complexes. These conclusions are supported by the $^{31}P\{^1H\}$ NMR data (*vide infra*). The Raman spectra also show strong bands at 85, 56 and 45 cm^{-1} which can be assigned to the $\delta(HgX_2)$ bending modes

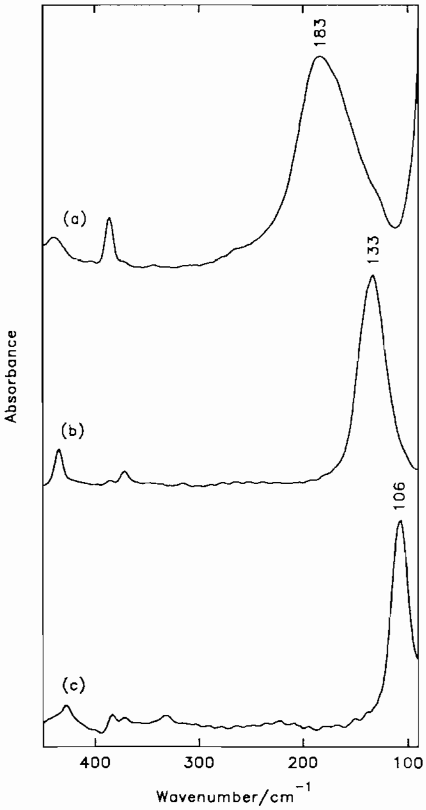

Fig. 5. Far-IR spectra of $(PEt_3)_2HgX_2$; (a) X = Cl, (b) X = Br, (c) X = I.

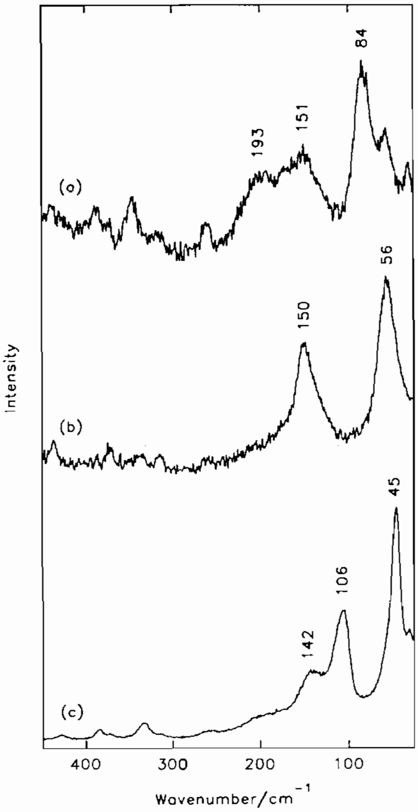

Fig. 6. Raman spectra of $(PEt_3)_2HgX_2$; (a) X = Cl, (b) X = Br, (c) X = I.

of the HgX_2 units in the complexes. These are reduced by a factor of about 0.8 relative to the values for the corresponding gas phase HgX_2 molecules. By contrast, the ν(HgX) wavenumbers are reduced by a factor of 0.45 relative to the ν_3 values for the corresponding gas phase HgX_2 molecules. This is similar to the situation recently described for the species $[(PPh_3)CuX_2]^-$, where the ν(CuX) wavenumbers are considerably lower than the ν_3 values for $[CuX_2]^-$, but the $\delta(CuX_2)$ values for corresponding species are almost the same [56]. The value of $\delta(HgCl_2) = 85$ cm^{-1} in $[(PEt_3)_2HgCl_2]$ is significantly lower than the value 110 cm^{-1} which has been reported for the corresponding PPh_3 complex [20].

Of the three possible $[(PBu_3)_2HgX_2]$ complexes, we could only obtain the X = Cl compound as a pure isolable solid. Its far-IR spectrum shows a strong ν(HgX) band at 205 cm^{-1}, and a band at 83 cm^{-1} which is assigned to the $\delta(HgCl_2)$ mode. The Raman spectrum obtained for this complex was of relatively poor quality, but a ν(HgX) band almost coincident with the IR band at 205 cm^{-1} was observed at 206 cm^{-1}. A weak band at 128 cm^{-1} in the Raman spectrum was assigned to a ν(HgP) mode and a strong band at 83 cm^{-1} in the far-IR spectrum was assigned to the $\delta(HgCl_2)$ mode, by analogy with similar assignments for related complexes discussed above.

The close similarities between the results for the above complexes suggest that they all have structures which are the same as those which have already been determined for the PPh_3 complexes [4, 11] and for $[(PEt_3)_2HgCl_2]$ [7], and this was proved in the present study by the X-ray crystallographic structure determination for $[(DBP)_2HgBr_2]$ (*vide supra*). Complexes $[L_2HgX_2]$ with this structure should in principle give two ν(HgX) and two ν(HgP) modes, all of which are active in both the IR and the Raman spectra. However, this was only observed in the present study for the ν(HgX) modes, and then only for the cases L = PPh_3, DBP with X = Cl. In all other cases, the symmetric and antisymmetric stretching modes must be so close in wavenumber that they remain unresolved.

For the complexes $[(PEt_3)_2HgX_2]$ it was noted above that the ratio of ν(HgX) to the ν_3 value for the corresponding gas phase HgX_2 molecule is 0.45 for all three complexes X = Cl, Br, I. The reduction in the wavenumber of this band on complex formation is an indication of the strength of the Hg–P bonds which are formed, and the above ratio can be used as a quantitative indicator of the relative Hg–P bond strengths with different phosphine ligands. The values of these ratios for the ligands studied in this work are 0.54 (PPh_3), 0.56 (DBP), 0.55 (DMPP), 0.45 (PEt_3)

and 0.50 (PBu_3; from data for X = Cl only). This emphasizes the considerably greater donor strength of PEt_3 relative to the other ligands, and suggests that the donor strength of PBu_3 lies midway between that of PEt_3 and those of the group PPh_3, DBP and DMPP, all of which are relatively close. A previously reported attempt to correlate ligand basicity with vibrational spectroscopic parameters was unsuccessful, and it was concluded that extensive coupling of vibrational modes masked any such trends which might have been present [20]. However, the ligands used in that study were closely related, all being derivatives of PPh_3. The present results show that the vibrational spectra do correlate with the ligand basicity when phosphines with a greater range of basicities are studied, but not with pK_as of the phosphines [57] which are 8.69 (PEt_3), 8.43 (PBu_3), 2.73 (PPh_3), 0.5 (DBP) [58].

1:1 Complexes

The IR and Raman spectra of $[(PPh_3)_2Hg_2X_4]$ have been reported previously [9, 17, 18], and have been assigned on the basis of the symmetrical dimer structure (type **A** above) which had been determined for the X = Cl, I cases [5, 16]. For a centrosymmetric structure, group theory predicts one ν(HgP), one $\nu(HgX_t)$ and two $\nu(HgX_b)$ in the IR and Raman spectra, with mutual exclusion between IR and Raman. When the inversion centre is lost, as in the case of $[(PPh_3)_2Hg_2X_4]$ (X = Br, I) in the solid state (*vide supra*), the number of possible bands is doubled and all of them should be both IR and Raman active. The situation observed experimentally never corresponds to either of these cases. For example, for the case of $[(PPh_3)_2Hg_2Cl_4]$ which has a centrosymmetric structure, no $\nu(HgX_b)$ bands are observed in the Raman, and two $\nu(HgX_t)$ bands are observed in the IR (Table 11). This splitting of the single band expected on the basis of the structure of the asymmetric unit is due to correlation field effects, and is quite small (3 cm^{-1}). This can be contrasted with the larger splittings of 13 and 24 cm^{-1} observed in the $\nu(HgX_t)$ bands in the IR spectra of the Br and I analogues, which are not centrosymmetric. In the latter compounds, only three of the four expected $\nu(HgX_b)$ bands are observed, but there is a mutual exclusion between the IR and Raman spectra, as would be expected for a centrosymmetric structure. Thus, the vibrational spectra do not give a very clear indication of the exact symmetry of the dimer. This can be contrasted with the solid state NMR results (*vide infra*), which allow an unambiguous distinction to be made between the centrosymmetric and non-centrosymmetric structures.

The results for the complexes $[(DBP)_2Hg_2X_4]$ and $[(DMPP)_2Hg_2X_4]$ further illustrate this limitation. Of these compounds, only $[(DBP)_2Hg_2Cl_4]$ and $[(DMPP)_2Hg_2I_4]$ show a splitting of the $\nu(HgX_t)$ band in the IR (8 and 7 cm^{-1}, respectively). This suggests that the others have centrosymmetric structures, and this agrees with the solid state NMR data. The crystal structure of $[(DMPP)_2Hg_2I_4]$ shows that this complex has a non-centrosymmetric structure, but the splitting of the $\nu(HgI_t)$ band is considerably smaller than in the corresponding PPh_3 complex, despite the fact that the differences in the lengths of the two Hg–I_t bonds are the same for the two cases (Table 8). The exact symmetry of $[(DBP)_2Hg_2Cl_4]$ cannot therefore be deduced from the IR spectrum, but the solid state NMR data suggest a centrosymmetric structure, so the splitting of $\nu(HgCl_t)$ in this case must be due to correlation field effects, as it is in the corresponding PPh_3 compound.

It was shown above that the 2:1 complexes with the DBP and DMPP ligands showed $\nu(HgX_t)$ bands which were slightly higher than those of the corresponding PPh_3 complexes, and that this correlates with a slightly shorter Hg–X bond length in the case of $[(DBP)_2HgBr_2]$. For the 1:1 complexes of DBP and DMPP, the trend appears to be in the opposite direction in all cases except for $[(DMPP)_2Hg_2I_4]$. This is the only member of these series for which a crystal structure determination was carried out and, indeed the Hg–I_t bond lengths in this compound are shorter than those in the PPh_3 analogue (Table 8). Presumably the opposite trend occurs for the other members of these series. $[(DMPP)_2Hg_2I_4]$ is thus unique in two respects; it is the only member of the 1:1 series of complexes with the phosphole ligands to have a non-centrosymmetric structure in the solid state, and it appears to be the only member for which the Hg–X_t bonding is stronger than the PPh_3 analogue.

It has previously been shown that the separation between the two IR active $\nu(HgX_b)$ modes in $[L_2Hg_2X_4]$ is related to the distortion of the central Hg_2X_2 ring from ideal D_{2h} symmetry [9]. This can be checked in the present study for the X = I complexes with L = PPh_3 or DMPP. The separation of the two IR active (HgI_b) modes in the PPh_3 case is 28 cm^{-1}, whereas only a single $\nu(HgI_b)$ band is seen in the DMPP case. The structural data (Table 8) show that the range of Hg–I_b bond lengths is indeed less in the DMPP complex, so that the central Hg_2X_2 ring is closer to ideal D_{2h} symmetry in this case. This result is similar to one obtained previously for $[L_4Ag_2Cl_2]$ with L = PPh_3 or DBP, where it was found that the two $\nu(AgCl_b)$ modes show a greater separation in the PPh_3 case, and this correlates with a greater degree of distortion in the Ag_2Cl_2 ring from D_{2h} symmetry [42].

The structure of the 1:1 PEt_3 complex of $HgCl_2$ has been determined [6] and the corresponding Br complex is isostructural [12]. The structure is a chain polymer which can be considered to consist of $[(PEt_3)_2Hg_2X_4]$

dimers which are linked together via additional, weaker Hg - - - X contacts. The far-IR and Raman spectra have been reported previously [9, 12], and the present results are in reasonable agreement with that data. The bands can be assigned in the same way as those for the other [$L_2Hg_2X_4$] species discussed above, and it has been pointed out that the additional Hg - - - X interactions which convert the structure from a dimeric to an infinite polymeric one appear to have remarkably little effect on the spectra [9].

The 1:1 complex of PBu_3 with $HgCl_2$ exists in two forms known as the α- and β-forms. The β-form contains discrete centrosymmetric [$(PBu_3)_2Hg_2Cl_4$] dimers [8], while the α-form consists of a tetrameric unit in which [$(PBu_3)_2Hg_2Cl_4$] dimers are linked together via additional, weaker Hg - - - Cl contacts [5]. The IR and Raman spectra of these two forms have been reported previously, and the present results are in reasonable agreement with these. The spectra of the two forms are distinctly different, that of the α-form being more complex and showing a less clear distinction between bands due to terminal and bridging bonds [8]. The spectra of the 1:1 complexes of PBu_3 with $HgBr_2$ and HgI_2 have also been reported previously, and have been interpreted in terms of a 'pseudo-tetramer' structure similar to that of the α-form of the $HgCl_2$ complex [12]. However, the crystal structure determination in the present study shows that the structure of the HgI_2 complex is not based on the symmetric dimer form **A**, but rather that it has the unsymmetrical structure **B** (*vide supra*). The close similarity in the appearance of the vibrational spectra of the Br and I complexes suggests that they are isostructural, and this is confirmed by the solid state NMR results (*vide infra*).

Solution ^{31}P NMR spectra

As previously reported [46] for the analogous [$(PR_3)_nCdX_2]_m$ complexes, the $^{31}P\{^1H\}$ NMR spectra of the [$(PR_3)_nHgX_2]_m$ complexes are temperature dependent. In general, the ^{31}P chemical shift moves to higher frequency, the linewidths narrow and resolution of coupling to ^{199}Hg ($I = 1/2$, 16.84%, $\gamma = 4.7690 \times 10^7$ rad T^{-1} s^{-1}) [59] occurs as the temperature decreases. The magnitudes of ^1J(HgP) also increase with decreasing temperature but not to as great an extent as found for ^1J(CdP). These spectral characteristics are indicative of exchange equilibria. For [$(DMPP)HgI_2]_2$, [$(DBP)HgBr_2]_2$ and [$(DBP)HgI_2]_2$ exchange could not be sufficiently slowed to observe phosphorus–mercury coupling at the lowest temperature that solubility would permit. The mercury complexes are more robust than the cadmium complexes and for many of the mercury complexes coupling may be observed at room temperature. For both cadmium and mercury the less soluble [$(PR_3)MX_2]_2$ complexes sometimes precipitate from solutions of the $(R_3P)_2MX_2$ complexes. This is particularly noticeable for $(DMPP)_2HgX_2$, and over a period of time $R_3P=0$ is formed in these solutions if they are exposed to air. This suggests that the exchange equilibria may be described largely by reaction (1).

$$(PR_3)_2MX_2 \rightleftharpoons (PR_3)MX_2 + PR_3 \qquad (1)$$

These equilibria are slow and generally lie far to the left such that the only species observed in the $^{31}P\{^1H\}$ NMR of solutions containing pure $(PR_3)_2HgX_2$ are the slowly exchanging $(PR_3)_2HgX_2$ complexes. Mixtures of $(PR_3)_2HgX_2$ and [$(PR_3)HgX_2]_2$ show separate resonances for each species with ^{199}Hg satellites for both resonances. Low temperature limiting data are given in Tables 12 and 13. As noted by previous workers [23, 25], ^1J(HgP) increases in the orders $I < Br < Cl$ and $(PR_3)_2HgX_2 < [(PR_3)HgX_2]_2$ and ^1J(HgP) correlates with the coordination chemical shift defined as

TABLE 12. 121.66 MHz $^{31}P\{^1H\}$ NMR data for $(PR_3)_2HgX_2$ complexes in $CDCl_3/CH_2Cl_2$ (1:1)

T	PR_3	X	$\delta^{31}P$ (ppm)	$\Delta\delta^{31}P$ (ppm)	$^1J(^{199}Hg^{31}P)$ (Hz)
230	PEt_3	Cl	37.90	57.90	5109.9
230	PEt_3	Br	32.27	52.27	4829.1
230	PEt_3	I	17.92	37.92	4153.0
230	PBu_3	Cl	28.96	61.46	5129.4
213	PPh_3	Cl	27.71	33.71	4766.1
213	PPh_3	Br	21.29	27.29	4240.3
243	PPh_3	I	6.10	12.10	3055.3
213	DMPP	Cl	26.23	28.73	4465.4
213	DMPP	Br	21.47	23.97	3886.1
208	DMPP	I	8.32	10.82	2509.5
213	DBP	Cl	16.58	27.58	4081.0
213	DBP	Br	8.65	19.65	3394.6
213	DBP	I	−8.62	2.38	2234.3

TABLE 13. 121.66 MHz $^{31}P\{^1H\}$ NMR data for [$(PR_3)HgX_2]_2$ complexes in $CDCl_3/CH_2Cl_2$ (1:1)

T	PR_3	X	$\delta^{31}P$ (ppm)	$\Delta\delta^{31}P$ (ppm)	$^1J(^{199}Hg^{31}P)$ (Hz)
230	PEt_3	Cl	80.35	100.35	7451.2
230	PEt_3	Br	74.36	94.36	6718.7
230	PEt_3	I	52.80	72.80	5273.5
233	PBu_3	Cl	33.12	65.62	7460.9
233	PBu_3	Br	27.55	60.05	6743.2
223	PBu_3	I	6.27	38.77	5342.7
213	PPh_3	Cl	33.63	39.63	7670.2
181	PPh_3	Br	26.64	32.64	6450.0
213	PPh_3	I	6.42	12.42	4774.4
233	DMPP	Cl	28.52	31.02	7180.2
181	DMPP	Br	24.89	27.39	6352.6
185	DMPP	I	9.56	12.06	unresolved
213	DBP	Cl	22.06	32.06	7424.5
185	DBP	I	−2.36	13.36	unresolved

$\Delta\delta = \delta^{31}$P(complex) $- \delta^{31}$P(ligand). These trends have been explained [23, 25] on the basis of an increase in the mercury–phosphorus bond strength giving rise to an increase in both ^{1}J(HgP) and $\Delta\delta$. For the $(PR_3)_2HgX_2$ complexes we find good correlations between $\Delta\delta$ and ^{1}J(HgP) that divide into two sets: $(PEt_3)_2HgX_2$ ($\Delta\delta = 0.0209 \times {}^{1}J(\text{HgP}) - 49.0148$, $r^2 = 0.99$) and all other $(PR_3)_2HgX_2$ complexes ($\Delta\delta = 0.0153 \times {}^{1}J(\text{HgP}) - 33.0825$, $r^2 = 0.84$). The separation of the PEt_3 complexes is consistent with the conclusions derived from the vibrational spectroscopy data that the donor ability of PEt_3 toward mercury(II) is much greater than that of the other phosphines studied. It should be pointed out however, that the data for $(PBu_3)_2HgCl_2$ are more similar to those of $(PEt_3)_2HgX_2$ than to those of the other phosphine complexes (see Fig. 7). Furthermore, the reported data [23, 27] for $(PBu_3)_2HgX_2$ (X = Br, I) when plotted in the same way would suggest that PBu_3 is a better donor than PEt_3, a conclusion that is not supported by the vibrational spectroscopy data.

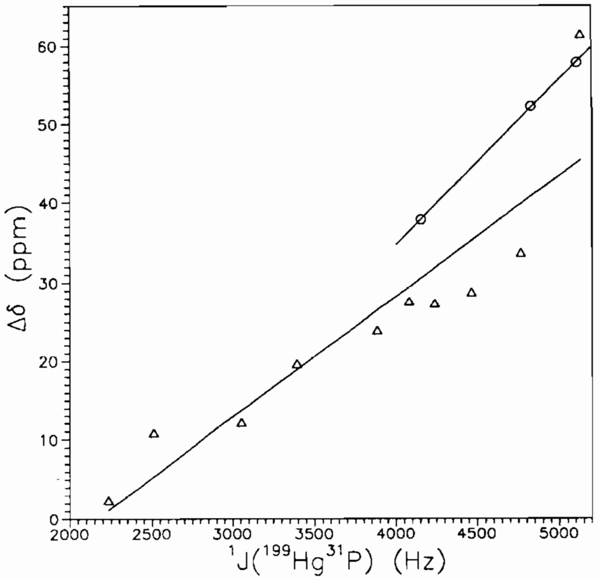

Fig. 7. Correlation of $\Delta\delta$ with ^{1}J(HgP) for $(PEt_3)_2HgX_2$ (○) and all other $(PR_3)_2HgX_2$ (△) complexes.

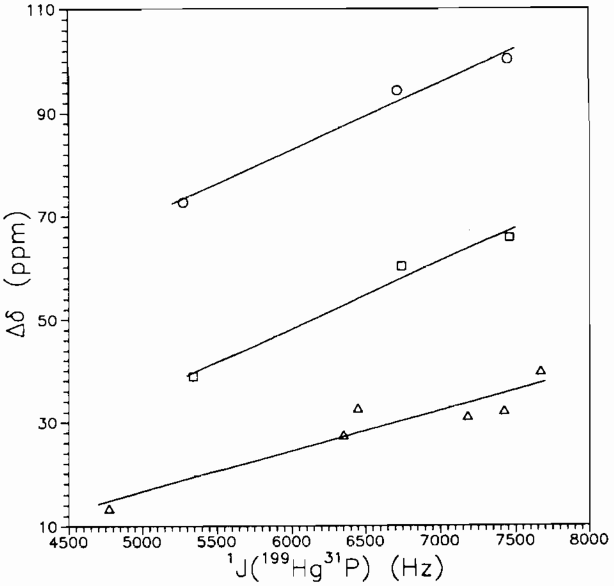

Fig. 8. Correlation of $\Delta\delta$ with ^{1}J(HgP) for $[(PEt_3)HgX_2]_2$ (○), $[(PBu_3)HgX_2]_2$ (□) and all other $[(PR_3)HgX_2]_2$ (△) complexes.

Similar correlations of $\Delta\delta$ with ^{1}J(HgP) exist for the $[(PR_3)HgX_2]_2$ complexes (Fig. 8) but now divide into three groups: $[(PEt_3)HgX_2]_2$ ($\Delta\delta = 0.01297 \times {}^{1}J(\text{HgP}) + 5.123$, $r^2 = 0.98$); $[(PBu_3)HgX_2]_2$ ($\Delta\delta = 0.01302 \times {}^{1}J(\text{HgP}) - 30.0312$, $r^2 = 0.98$); and all other $[(PR_3)HgX_2]_2$ complexes ($\Delta\delta = 0.00777 \times {}^{1}J(\text{HgP}) - 22.2656$, $r^2 = 0.88$). Alyea *et al.* [25] found similar divisions for complexes of PCy_3, PBu^t_3 and P (*o*-tolyl)$_3$. The slopes of these correlations for the $[(PEt_3)HgX_2]_2$ and $[(PBu_3)HgX_2]_2$ complexes are essentially the same and roughly twice that for the other correlation. It is known that ^{1}J(HgP) [29, 30] and ^{1}J(CdP) [46] depend upon bond angles at the metal and increase as the PHgP angle increases for $(PR_3)_2HgX_2$ complexes. Of this basis one would expect ^{1}J(HgP) for $(DBP)_2HgBr_2$ (PHgP = 119.4°) to be larger than for $(Ph_3P)_2HgBr_2$ (PHgP = 113.0°) but in fact the coupling for the former is 845 Hz less than that for the latter. This behaviour may be compared to what we found [46] for analogous cadmium complexes: $(Ph_3P)_2CdI_2$ (PCdP = 105.1°, ^{1}J(CdP) = 917 Hz (ave)); $(DBP)_2CdI_2$ (PCdP = 97.5°, ^{1}J(CdP) = 915 Hz. We find no linear relationship between ^{1}J(HgP) and the PHgP angle for the eleven compounds for which the data have been reported though for constant halide ^{1}J(HgP) does decrease as the PHgP angle decreases. Since the PHgP angle should be a function of ligand steric bulk it appears that ^{1}J(HgP) is not a simple function of ligand steric bulk. According to Brown's [60] recent calculations of ligand steric effects PEt_3 and PBu_3 have very similar steric bulk ($E_R = 61$ and 64, respectively) and are less sterically encumbered than PPh_3 ($E_R = 75$), PCy_3 ($E_R = 116$) and PBu^t_3 ($E_R = 154$). The value of ^{1}J(HgP) for the $[(PR_3)_2HgX_2]_2$ complexes is very much dependent upon the nature of the halide but not much on the nature of the phosphine. For the $(PR_3)_2HgX_2$ complexes ^{1}J(HgP) is somewhat more sensitive to the nature of the phosphine. As shown by crystallographic data [5–16] the bond angles at the metal depend strongly upon the halide and the phosphine. For the $[(PR_3)HgX_2]_2$ complexes the ^{1}J(HgP) values are very similar for constant X and phosphines of widely different basicities but $\Delta\delta$ is strongly dependent on both the halide and the phosphine. It ($\Delta\delta$) increases slightly with decreasing steric bulk ($PPh_3 > DBP > PBu_3 \sim PEt_3$) and strongly with increasing phosphine basicity ($DMPP \sim DBP < PPh_3 < PBu_3 < PEt_3$). For these complexes then, ^1J(HgP) is dominated by electronic effects and $\Delta\delta$ is a function of both electronic and steric effects. Thus, for the $(PR_3)_2HgX_2$ complexes a steric threshold appears to be reached for ligands more bulky than PEt_3 or PBu_3 and for the $[(PR_3)HgX_2]_2$ complexes no steric threshold has been reached. Consequently, $\Delta\delta$ is more dependent on phosphine basicity for the sterically less encumbered $[(PR_3)HgX_2]_2$ complexes and on ligand steric bulk for the more encumbered $(PR_3)_2HgX_2$ complexes.

The $[(PBu_3)HgI_2]_2$ complex deserves special comment. As isolated, the solid contains two crystalline phases. The major phase is the unsymmetrical dimer (form **B**) and the minor phase is probably the symmetrical dimer (form **A**). Grim *et al.* [23] suggested that in solution there was a 60:40 ratio of form **A** to form **B**. Goggin *et al.* [26] and Colton and Dakternieks [27] have shown that form **B** is favored by increasing concentration. We obtained the spectra of the $[(PBu_3)HgX_2]_2$ complexes on dilute ($\sim 10^{-3}$ M) solutions at low temperature where the $^{31}P\{^1H\}$ NMR data are consistent with essentially only the symmetric dimers being present in each case [27] (note the correlation in Fig. 8).

CP/MAS ^{31}P NMR spectra

The ^{31}P NMR parameters obtained from an analysis of the CP/MAS ^{31}P NMR spectra are listed in Table 14, and some typical spectra are shown in Figs. 9 and 10.

2:1 Complexes

The spectra of the 2:1 PPh_3 complexes $[(PPh_3)_2HgX_2]$ have been reported previously [21], and the results obtained in the present study are in reasonable agreement with these. In all three complexes, the two phosphorus atoms are inequivalent, and show different ^{31}P chemical shifts and $^1J(^{199}HgP)$ coupling constants. There is also a ^2J(PP) coupling between the inequivalent P atoms, so that the ^{199}Hg satellite structure consists of a pair of AB patterns which are the AB part of an ABX spin system (A, B $=$ ^{31}P; X $=$ ^{199}Hg). The 2:1 DBP complexes show exactly analogous behaviour, but the DMPP complexes show only a single ^{31}P chemical shift, implying that the two P atoms in the molecule are structurally equivalent in the solid. The ^{199}Hg satellite structure simply consists of a doublet which is the A part of an A_2X spin system. The 2:1 PEt_3 complexes show ABX patterns in the case of the Br and I compounds, implying that the two P atoms are inequivalent in the solid. However, the Cl complex shows the A_2X pattern characteristic of two equivalent P atoms (Fig. 9). This agrees with the previously reported crystal structure [7] in which the two PEt_3 ligands are crystallographically identical. The complex $[(PBu_3)_2HgCl_2]$ shows the ABX pattern, indicating that the P atoms are inequivalent.

1:1 Complexes

The structures of $[(PPh_3)_2Hg_2I_4]$ (X $=$ Cl, I) [5, 16] and X $=$ Br (this work) are known. Whereas the X $=$ Cl compound has a centrosymmetric structure, the X $=$ Br, I complexes have non-centrosymmetric structures in which the Hg and P atoms are inequivalent (*vide supra*). For the centrosymmetric structure, both Hg–P bonds are symmetrically equivalent, and are too far apart in the molecule to allow any magnetic interaction. The ^{199}Hg satellite structure thus consists of a single doublet which is the A part of an AX spin system. For the non-centrosymmetric structure, the two Hg–P bonds are inequivalent, resulting in two different AX spin systems. The ^{199}Hg satellite structure thus consists of two doublets. The observed spectra for the 1:1 PPh_3 complexes conform exactly to these predictions, showing a single AX pattern for the centrosymmetric Cl complex, and two AX patterns for the Br and I complexes. This unambiguous result can be compared with the situation for the vibrational spectra, where the observed number of lines never corresponds to the predictions based on the structure of the asymmetric unit in the solid.

The results for $[(DBP)_2Hg_2X_4]$ (X $=$ Cl, Br, I) and $[(DMPP)_2Hg_2X_4]$ (X $=$ Cl, Br) (a single AX pattern is observed for each of these), indicate that these complexes have centrosymmetric structures in the solid.

The spectrum of $[(DMPP)_2Hg_2I_4]$ (**3**) shows three AX patterns (Fig. 10). This is not compatible with the crystal structure of this complex (*vide supra*), which shows a non-centrosymmetric structure for which two AX patterns are expected. Apparently this compound can crystallize in two forms, a minor centrosymmetric form (30%) and a major non-centrosymmetric form (70%) and the major form was selected for the structure determination (see 'Experimental').

As discussed above, the 2:1 complex of PBu_3 with $HgCl_2$ exists in two forms known as the α- and β-forms. The β-form contains discrete centrosymmetric $[(PBu_3)_2Hg_2Cl_4]$ dimers [8], while the α-form consists of a tetrameric unit in which $[(PBu_3)_2Hg_2Cl_4]$ dimers are linked together via additional, weaker Hg - - - Cl contacts [5]. For the β-form, a single AX pattern is expected as discussed above, while for the α-form there are two sets of two inequivalent Hg–P bonds in the 'pseudo-tetramer', so that two AX patterns of equal intensity are expected. Only in the case of the α-form was it possible to prepare sufficient sample for a solid state NMR study, and this showed the two equal AX patterns, as expected (Fig. 11).

The 2:1 complexes of PBu_3 with $HgBr_2$ and HgI_2 each show two sets of ABX patterns (Fig. 11). The ABX spectrum immediately indicates the presence of

TABLE 14. ^{31}P CP/MAS NMR parameters for L_nHgX_2

L	n	X	Spin system	$\delta(^{31}P)$ (ppm)		$^1J(^{199}HgP)$ (Hz)		$^2J(PP)$ (Hz)
				δ_A	δ_B	J_{AX}	J_{BX}	J_{AB}
PPh_3	1	Cl	AX	39.6		7448		
	1	Br	AX	33.8		6264		
			AX	35.4		6611		
	1	I	AX	11.9		4428		
			AX	14.8		4957		
	2	Cl	ABX[a]	27	27	4600	4600	180
	2	Br	ABX	13.0	18.5	4182	3183	164
	2	I	ABX	2.0	6.8	2644	2330	154
DBP	1	Cl	AX	28.0		7328		
	1	Br	AX	20.3		6219		
	1	I	AX	−1.3		4423		
	2	Cl	ABX	13.4	19.1	3580	4499	198
	2	Br	ABX	5.6	11.8	3185	3981	152
	2	I	ABX	−6.4	−11.7	2119	1968	115
DMPP	1	Cl	AX	31.0		7883		
	1	Br	AX	24.2		6944		
	1	I	AX	17.7		4615		
			AX	17.7		4615		
			AX	23.1		4578		
	2	Cl	A_2X	22.2		3723		
	2	Br	A_2X	17.2		3345		
	2	I	A_2X	6.1		2642		
PEt_3	1	Cl	AX	46.9		7928		
	1	Br	AX	38.8		7028		
	1	I	AX	21.5		5268		
	2	Cl	A_2X	44.9		5287		
	2	Br	ABX	32.9	34.7	4579	4445	166
	2	I	ABX	20.4	21.5	4007	4141	120
PBu_3	1	Cl	AX	37.2		7285		
			AX	38.2		7344		
	1	Br	ABX	34.4	37.0	5111	5175	173
			ABX	36.3	38.3	4833	4911	182
	1	I	ABX	19.4	23.7	5032	5102	147
			ABX	22.2	25.3	4691	4793	158
	2	Cl	ABX	30.1	35.1	4621	4826	170

[a] Spectrum too noisy to allow accurate analysis.

two inequivalent P atoms attached to the same Hg atom. The presence of two ABX patterns indicates that there are two such HgP_2 units which are symmetrically inequivalent, and which are sufficiently well separated that they do not interact magnetically. The crystal structure of the HgI_2 complex shows how this arises. The complex consists of dimers with the unsymmetrical structure **B**, in which both of the phosphine molecules are attached to the same Hg atom. Moreover, there are two such molecules in the asymmetric unit, which explains the presence of two distinct ABX patterns in the spectrum. The fact that the $HgBr_2$ complex shows exactly the same kind of spectrum confirms the conclusion reached above on the basis of the vibrational data, namely that it is isostructural with the HgI_2 complex.

The results of the present study and those of the previous study of the analogous cadmium(II) complexes [46] provide CP/MAS ^{31}P NMR data for a number of isostructural cadmium(II) and mercury(II) complexes, and this allows a comparison to be made of the ^1J(MP) coupling constants for these complexes. These parameters are listed in Table 15. In order to eliminate the effect of the different magnetic moments of the metal nuclei on these coupling constants, they have been divided by the magnetogyric ratio γ of the metal nucleus concerned (the γ value used for Cd is the weighted mean for the naturally occurring isotopes ^{111}Cd, 12.75%, and ^{113}Cd, 12.26%, since separate signals were not always observed for the two isotopes). This yields a reduced coupling constant J_r, which is essentially the magnitude of the magnetic field at the metal nucleus,

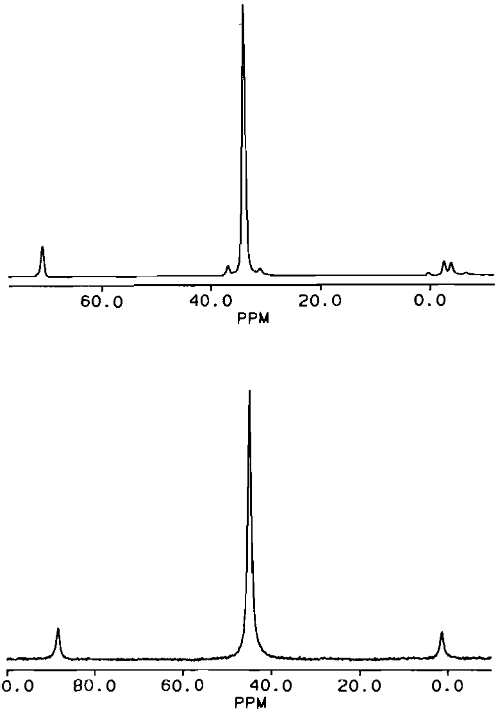

Fig. 9. 60.74 MHz CP/MAS $^{31}P\{^1H\}$ NMR spectra of $(PEt_3)_2HgBr_2$ (upper) and $(PEt_3)_2HgCl_2$ (lower).

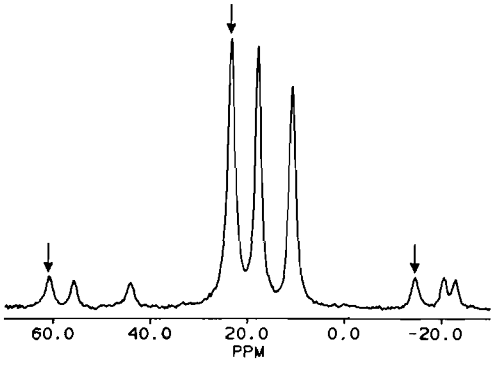

Fig. 10. 60.74 MHz CP/MAS $^{31}P\{^1H\}$ NMR spectrum of $[(DMPP)HgI_2]_2$. Resonances due to the minor form are marked with arrows.

which is induced by the magnetic moment of the phosphorus nucleus by means of the Fermi contact interaction between the nuclei and the electrons in the M–P bond. Since this arises from the Fermi contact interaction it depends on the contributions of the phosphorus and the metal S orbitals to the M–P bonds. The cadmium and mercury complexes that are compared in Table 15 have the same phosphorus donor ligands, so the phosphorus s-orbital contribution should be similar in both cases. Thus, the values of J_r should be dominated by the metal s-orbital involvement in the M–P bond (but see the recent discussion by Power and Wasylishen [61] for ${}^1P$(PtP)). The results in Table 15 show that the J_r values for the mercury complexes are a factor of 3.6 ± 0.9 greater than those of the corresponding cadmium complexes. This suggests that the metal s-orbital involvement in the M–P bond is greater for Hg than for Cd. For those complexes which have been characterized by X-ray crystallography, one can calculate [62] the s- and p-orbital involvement assuming sp^{λ^2} hybridization from the bond angles about the metal from the equations: $\lambda^2 = -1/\cos\theta$; $\%s = 100/(1+\lambda^2)$; $\%p = 100 - \%s$. Thus, for $(DBP)_2CdI_2$ ($PCdP = 97.5°$, $\%s = 11.6$); $(Ph_3P)_2CdI_2$ ($PCdP) = 105.1°$, $\%s = 20.7$); $(Ph_3P)_2CdCl_2$ ($PCdP = 107.6°$, $\%s = 23.2$); $(PEt_3)_2HgCl_2$ ($PHgP) = 158.5°$, $\%s = 48.2$); $(Ph_3P)_2HgCl_2$ ($PHgP) = 134.1°$, $\%s = 41.0$); $(DBP)_2HgBr_2$ ($PHgP = 119.4°$, $\%s = 32.9$); $(PPh_3)_2HgBr_2$ ($PHgP) = 113.0°$, $\%s = 28.1$); $(PPh_3)_2HgI_2$ ($PHgP = 109.95°$, $\%s = 25.4$) (see refs. 21

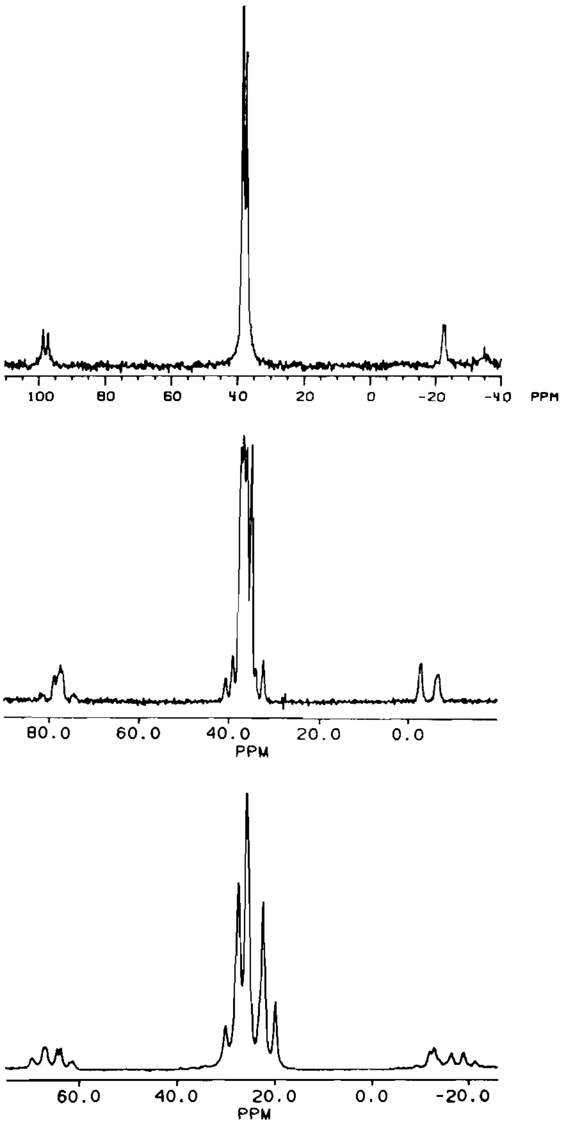

Fig. 11. 60.74 MHz CP/MAS $^{31}P\{^1H\}$ NMR spectra of $[(PBu_3)HgX_2]_2$; X = Cl (top), X = Br (middle), X = I (bottom).

TABLE 15. Comparison of ^1J(MP) values from CP/MAS $^{31}P\{^1H\}$ NMR spectra of isostructural cadmium(II) and mercury(II) complexes with phosphorus donor ligands[a]

Complex		J (Hz)		$10^6J_r/T$[b]		R[c]
		M=Cd	M=Hg	M=Cd	M=Hg	
$(PR_3)_2MX_2$						
PEt_3	Cl	1490	5287	25.7	110.9	4.32
PEt_3	Br	1430	4512	24.7	94.6	3.83
PEt_3	I	1333	4074	23.0	85.4	3.71
DMPP	Cl	1287	3723	22.2	78.1	3.52
DMPP	Br	1166	3345	20.1	70.1	3.49
DMPP	I	1032	2642	17.8	55.4	3.13
DBP	Cl	1356	4040	23.4	84.7	3.62
DBP	Br	1184	3583	20.4	75.1	3.68
DBP	I	915	2044	15.8	42.9	2.72
PPh_3	Cl	1381	4600	23.8	96.5	4.05
PPh_3	Br	1340	3683	23.1	77.2	3.34
PPh_3	I	767	2487	13.2	52.1	3.95
$[(PR_3)HgX_2]_2$						
PEt_3	Cl	2447	7928	42.2	166.2	3.94
PEt_3	Br	2307	7028	39.8	147.4	3.70
PEt_3	I	1768	5268	30.4	110.5	3.63
DMPP	Cl	2067	7883	35.6	165.3	4.64

[a]Data for the mercury compounds from this work data for the cadmium compounds from ref. 46. Average values where more than one J(MP) is observed. [b]$J_r = |J/\gamma|\gamma/10^7 T^{-1}\ s^{-1} = -5.7997$ (^{111,113}Cd), 4.7690 (^{199}Hg). [c]$R = J_r(\mathrm{Hg})/J_r(\mathrm{Cd})$.

and 29 for similar calculations). The data in Table 15 show that for a given metal ^1J(MP) generally increases with increasing metal s character in the hybrid orbitals. One would expect that the relative s-orbital participation for Cd and Hg would depend upon the relative s–p orbital energy separation. A large energy separation should lead to a greater participation of the s-orbitals in the bonding [63]. For Group 12 metal monocations this energy difference is 6.07, 5.68 and 7.14 eV for Zn, Cd and Hg, respectively [64]. The order deduced from the ^1J(MP) values is Hg > Cd which is similar to what we previously [42] observed for Ag > Cu and is consistent with a general increase in s-electron density with an increase in the mass of M [65].

For both the cadmium and mercury complexes the values of ^2J(PP) decrease in the sequence Cl > Br > I and this generally corresponds to a decrease in the PMP angle. Thus, it appears that for the complexes $(PR_3)_2MX_2$, M = Cd, Hg, δ^{113}Cd, δ^{199}Hg, ^1J(CdP), ^1J(HgP) and ^2J(PP) are all related to the PMP angle.

Supplementary material

For the crystal structure studies, crystal and refinement data, H atoms coordinates, thermal parameters and bond distances and angles have been deposited with the Cambridge Crystallographic Data Centre. Listings of observed and calculated structure factors are available from the authors.

Acknowledgements

The financial support of the UNR Research Advisory Board, the donors of the Petroleum Research Fund, administered by the American Chemical Society, the New Zealand Grants Committee, the University of Auckland Research Committee, and the National Science Foundation (Grant No. CHE-8616437) to the Colorado State University NMR Center is gratefully acknowledged. We thank Dr John Seakins for recording the Raman spectra.

References

1 R.C. Evans, F.G. Mann, H.S. Peiser and D.J. Purdie, *J. Chem. Soc.*, 1209 (1940).
2 C.A. McAuliffe (ed.), *Transition Metal Complexes of Phosphorus, Arsenic and Antimony Ligands,* Macmillan, London, 1973; C.A. McAuliffe and W. Levason, *Phosphine, Arsine and Stibine Complexes of the Transition Elements,* Elsevier, Amsterdam, 1979.
3 P.A.W. Dean, *Prog. Inorg. Chem. 24* (1978) 109.
4 L. Falth, *Chem. Scr., 9* (1976) 71.
5 N.A. Bell, M. Goldstein, T. Jones and I.W. Nowell, *Inorg. Chim. Acta, 43* (1980) 87.
6 N.A. Bell, M. Goldstein, T. Jones and I.W. Nowell, *Inorg. Chim. Acta, 48* (1981) 185.
7 N.A. Bell, T.O. Dee, P.L. Goggin, M. Goldstein, R.J. Goodfellow, T. Jones, K. Kessler, D.M. McKewan and I.W. Nowell, *J. Chem. Res. S, 2* (M) (1981) 201.
8 N.A. Bell, M. Goldstein, T. Jones, L.A. March and I.W. Nowell, *Inorg. Chim. Acta, 61* (1982) 83.
9 N.A. Bell, M. Golstein, T. Jones and I.W. Nowell, *Inorg. Chim. Acta, 69* (1983) 155.
10 N.A. Bell, T.D. Dee, M. Goldstein and I.W. Nowell, *Inorg. Chim. Acta,, 70* (1983) 215.
11 N.A. Bell, T.D. Dee, M. Goldstein, P.J. McKenna and I.W. Nowell, *Inorg. Chim. Acta, 71* (1983) 135.
12 N.A. Bell, M. Goldstein, T. Jones and I.W. Nowell, *Inorg. Chim. Acta, 75* (1983) 21.
13 N.A. Bell, M. Goldstein, L.A. March and I.W. Nowell, *J. Chem. Soc., Dalton Trans.,* (1984) 1621.
14 D.W. Allen, N.A. Bell, S.T. Fong, L.A. March and I.W. Nowell, *Inorg. Chim. Acta, 99* (1985) 157.
15 N.A. Bell, N.A. Chudley, L.A. March and I.W. Nowell, *Inorg. Chim. Acta, 141* (1988) 155.
16 N.A. Bell, L.A. March and I.W. Nowell, *Inorg. Chim. Acta, 156* (1989) 201.
17 G.B. Deacon, J.H.S. Green and D.J. Harrison, *Spectrochim. Acta, Part A, 24* (1968) 1921.
18 T. Allman, R.G. Goel and P. Pilon, *Spectrochim. Acta, Part A, 35* (1979) 923.
19 R.G. Goel, W.P. Henry and N.K. Jha, *Inorg Chem., 21* (1982) 2551.
20 T. Allman and R.S. Goel, *Can. J. Chem., 62* (1984) 615.
21 T. Allman and R.E. Lenkinski, *Inorg. Chem., 25* (1986) 3202.

22 R.L. Keiter and S.O. Grim, *Chem. Commun.,* (1968) 512.

23 S.O. Grim, P.J. Lui and R.L. Keiter, *Inorg. Chem., 13* (1974) 342.

24 S.O. Grim, D.P. Shaw, C.K. Haas, J.M. Ressmer and P.H. Smith, *Inorg. Chim. Acta, 36* (1979) 139.

25 E.C. Alyea, S.A. Dias, R.G. Goel, W.O. Ogini, P. Pilon and D.W. Meek, *Inorg. Chem., 17* (1978) 1697.

26 P.L. Goggin, R.J. Goodfellow, D.M. McEwan and K. Kessler, *Inorg. Chim. Acta, 44* (1980) L111.

27 R. Colton and D. Dakternieks, *Aust. J. Chem., 33* (1980) 955.

28 R. Colton and D. Dakternieks, *Aust. J. Chem., 34* (1981) 323.

29 H.B. Buergi, R.W. Kunz and P.S. Pregosin, *Inorg. Chem., 19* (1980) 3707.

30 H.B. Buergi, E. Fischer, R.W. Kunz, M. Parvez and P.S. Pregosin, *Inorg. Chem., 21* (1982) 1246.

31 R.W. Kunz, P.S. Pregosin, M. Camalli, F. Caruso and L. Zambonelli, *Helv. Chim. Acta, 66* (1983) 1661.

32 F. Mathey, *Top. Phosphorus Chem., 10* (1980) 1.

33 F. Mathey, J. Fischer and J.H. Nelson, *Struct. Bonding (Berlin), 55* (1983) 153.

34 J. H. Nelson and F. Mathey, in J.G. Verkade and L.P. Quin (eds.), *Phosphorus-31, NMR Spectroscopy in Stereochemical Analysis,* VCH, Deerfield Beach, FL, 1987, pp. 665–694.

35 F. Mathey, *Chem. Rev., 88* (1988) 429.

36 F. Mathey, *Angew. Chem., Int. Ed. Engl., 26* (1987) 275.

37 S. Affandi, J.H. Nelson, N.W. Alcock, O.W. Howarth, E.C. Alyea and G. Sheldrick, *Organometallics, 7* (1988) 1724, and refs. therein.

38 E.C. Alyea, J. Malito and J.H. Nelson, *Inorg. Chem., 26* (1987) 4294.

39 S. Attar, W.H. Bearden, N.W. Alcock, E.C. Alyea and J.H. Nelson, *Inorg. Chem., 29* (1990) 425.

40 S. Attar, J.H. Nelson, W.H. Bearden, N.W. Alcock, L. Solujic' and E.B. Milosavljevic', *Polyhedron, 10* (1991) 1939.

41 S. Attar, G.A. Bowmaker, N.W. Alcock, J.S. Frye, W.H. Bearden and J.H. Nelson, *Inorg. Chem., 30* (1991) 4743.

42 S. Attar, N.W. Alcock, G.A. Bowmaker, J.S. Frye, W.H. Bearden and J.H. Nelson, *Inorg. Chem., 30* (1991) 4166.

43 S. Affandi, R.L. Green, B.T. Hsieh, M.S. Holt, J.H. Nelson and E.C. Alyea, *Synth. React. Inorg. Met.-Org. Chem., 17* (1987) 307.

44 J.H. Nelson, S. Affandi, G.A. Gray and E.C. Alyea, *Magn. Reson. Chem., 25* (1987) 774.

45 G.A. Gray and J.H. Nelson, *Org. Magn. Reson., 14* (1980) 14.

46 J.M. Kessler, J.H. Reeder, R. Vac, C. Yeung, J.H. Nelson, J.S. Frye and N.W. Alcock, *Magn. Reson. Chem., 24* (1991) S94.

47 E.C. Alyea, J. Malito, S. Attar and J.H. Nelson, *Polyhedron, 11* (1992) 2409.

48 J.A. Davies and S. Dutremez, *Coord. Chem. Rev., 114* (1992) 61.

49 A. Breque, F. Mathey and P. Savignac, *Synthesis,* (1981) 983.

50 R.C. Evans, F.G. Mann, H.S. Peiser and D. Purdie, *J. Chem. Soc.,* (1940) 1209.

51 P.R. Brookes and B.L. Shaw, *J. Chem. Soc., Dalton Trans.,* (1974) 1702.

52 N. Walker and D. Stuart, *Acta Crystallogr., Sect. A, 39* (1983) 158.

53 *TEXAN-TEXRAY Structure Analysis Package,* Molecular Structure Corporation, 1985.

54 G.M. Sheldrick, *SHELXTL User Manual,* Nicolet, Madison, WI, 1981; 1986.

55 *International Tables for X-ray Crystallography,* Vol. IV, Kynoch, Birmingham, UK, 1974.

56 G.A. Bowmaker, Wang Jirong, R.D. Hart, A.H. White and P.C. Healy, *J. Chem. Soc., Dalton Trans.,* (1992) 787.

57 H.Y. Liu, K. Eriks, A. Prock and W.P. Giering, *Organometallics, 9* (1990) 1758.

58 L.D. Quin, J.G. Bryson and C.G. Moreland, *J. Am. Chem. Soc., 91* (1969) 3308.

59 R.K. Harris and B.E. Mann, *NMR and the Periodic Table,* Academic Press, New York, NY, 1978.

60 T.L. Brown, *Inorg. Chem., 31* (1992) 1986.

61 W.P. Power and R.E. Wasylishen, *Inorg. Chem., 31* (1992) 2176.

62 S.O. Grim, H.J. Plastas and C.L. Huheey, *Phosphorus Relat. Group V Elem., 1* (1971) 66.

63 R.S. Nyholm, *Proc. Chem. Soc.,* (1961) 273.

64 L.E. Orgel, *J. Chem. Soc.,* (1958) 4186.

65 J.G. Verkade and J.A. Mosbo, in J.G. Verkade and L.D. Quin (eds.), *Phosphorus-31 NMR spectroscopy in Stereochemical Analysis*, VCH, Deerfield Beach, FL, 1987, pp. 425–463.